Journal of Hydrology 659 (2025) 133316

Contents lists available at ScienceDirect

Journal of Hydrology

journal homepage: www.elsevier.com/locate/jhydrol

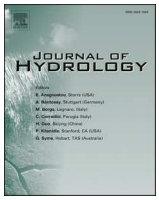

Research papers

A physically-informed long short-term memory-based tool for predicting extensive droughts in the distant future

Ali Ghaffari [a], Shrouq Abuismail [a], Y.C. Ethan Yang [a,*], Maryam Rahnemoonfar [a,b]

[a] Department of Civil and Environmental Engineering, Lehigh University, PA, USA
[b] Department of Computer Science & Engineering, Lehigh University, PA, USA

ARTICLE INFO

Keywords:
Combined drought index
3D drought clustering
Standardized precipitation index
US drought monitor
Crop management practices

ABSTRACT

Agricultural drought is a specific type of drought that impacts agricultural activities and crop yield by lower precipitation and shortages in soil water content. Developing a drought prediction tool is crucial as it can aid farmers and authorities in devising mitigation strategies like crop rotation and deficit irrigation. We developed a long-term, large-scale drought prediction tool solely based on remote-sensing data where drought intensity was measured by an enhanced combined drought index (ECDI) that utilized a weighted summation of four climatic variables: precipitation, temperature, Normalized Differenced Vegetation Index, and soil moisture. The State of Texas in the US is selected as our case study area. We trained a Long-Short Term Memory network with past 21 years of training data to predict the four climatic variables and calculated ECDI for the next 12 months. For model evaluation, we compared results of predicted droughts from ECDI to actual drought events based on SPI-3 (Standardized Precipitation Index with a three-month time scale). Results showed that ECDI and SPI exhibit similar spatial distribution of droughts but with different intensities. We also compared ECDI/SPI values to US Drought Monitor (USDM) maps which show experts' assessments of conditions related to dryness and drought. ECDI results were similar to USDM in case of drought extent but yielded different intensities. Results of this study showed that remote sensing data can be successfully used to predict future agricultural droughts for a longer period (12 months) and for a large-scale area to assist farmers and policymakers with designing mitigation measures.

1. Introduction

Agricultural drought refers to the impacts on agriculture by factors such as rainfall shortages, soil water deficits, reduced groundwater or reservoir levels needed for irrigation (National Weather Service, 2023). Recently, there has been a rise in both the number and severity of agricultural droughts in many parts of the world (Mishra & Singh, 2011). This increasing trend is because of higher temperatures due to climate change, shift in precipitation patterns, and limited and more competitive access to water resources (Damberg & AghaKouchak, 2014). Given that the changing climate condition is expected to continually affect the intensity, duration, and frequency of droughts (Parker et al., 2023), drought prediction becomes an even more complex task than before under the non-stationary climate. In the following lines, we explain the gaps in the literature that define the research question of this manuscript.

The first objective of this study is to address the issue of short forecast horizon in current drought prediction tools. The core of every drought prediction tool is the prediction module that forecasts climatic variables for a period into the future called forecast horizon. A longer forecast horizon is of crucial importance as it results in a longer lead time for authorities and farmers for planning ahead. This can help them strategize their plans for mitigation of drought impacts which can increase agricultural resilience to adverse growing conditions (Bowles et al., 2020). Current models use different approaches for the prediction module including SARIMA (seasonal autoregressive integrated moving average) (Kabbilawsh et al., 2022; Lu et al., 2018), and machine learning methods like CNN (convolutional neural networks) or LSTM (Meydani et al., 2022; Qiu et al., 2017; Sadeghi et al., 2019). However, the forecast horizon in most of the current models is not long enough for efficient implementation of crop management practices (Chang & Lin, 2019). Some of the current models are "nowcasting" models that predict climatic variables for the very near future (less than 24 h) which can only be used for drought monitoring and not prediction (Agrawal et al., 2019;

* Corresponding author.
E-mail address: yey217@lehigh.edu (Y.C.E. Yang).

https://doi.org/10.1016/j.jhydrol.2025.133316
Received 7 June 2024; Received in revised form 3 December 2024; Accepted 12 April 2025
Available online 14 April 2025

Shi et al., 2017). Other current models have a rather short forecast horizon (less than three months) with a focus on seasonal drought prediction (Akbari Asanjan et al., 2018; Gamboa-Villafruela et al., 2021; Luo et al., 2021; Meydani et al., 2021). These models cannot be applied for long-term planning and, therefore, are less effective when used for informing crop management mitigation practices such as crop rotation and soil cultivation which usually require a longer lead time (preferably twelve months or longer) (Chang & Lin, 2019). While some of the current models use a longer forecast horizon (more than twelve months), they emphasize on identifying trends in climatic variables without directly pointing to water availability or droughts especially agricultural droughts (T. Lee & Ouarda, 2010; Wang et al., 2022). To summarize, we observe a knowledge gap in current models to predict agricultural droughts in the distant future (at least twelve months) for early planning against drought impacts.

Our second objective is to improve the applicability of drought prediction tools for large-scale areas. Currently, most drought prediction tools are applied to a small case study area with a relatively homogenous climate (Kumar et al., 2021; Malik & Kumar, 2020; Nguyen et al., 2017). While these models offer detailed insights into drought dynamics at a local level (e.g., subbasin or county level), they are limited in meeting specific needs of authorities operating at larger scales (e.g., state or national level) (Mardian, 2022; Schwantes et al., 2018; Yazdandoost et al., 2022). Policy development and resource management strategies are achievable by large-scale models and the key to do so is by capturing the spatial variability in larger areas (Chen et al., 2014a; Wilhite et al., 2014). Spatial variability is shaped by multiple factors, including climate variability, changes in land use and cover, infrastructure developments (e.g., reservoirs), water extraction, and broader human interventions (Y. Li et al., 2024). These factors contribute to diverse drought propagation patterns (Tian et al., 2023) that have different impacts on various vegetation's health (Y. Zhang, Liu, et al., 2023). Therefore, an effective large-scale drought prediction tool must account for spatial variability for broader planning against agricultural droughts. Several studies have tried to capture spatial variability by using data that is consistently available at large scale. To include climate variability, some studies use one or multiple climatic variables (e.g., precipitation, temperature, and evapotranspiration) from remote sensing sources for drought monitoring (Safari et al., 2023; Vreugdenhil et al., 2022). To account for land cover variability, other studies use satellite-based vegetation indices such as NDVI (Normalized Differenced Vegetation Index which combines information from red and near-infrared spectral channels on a satellite to highlight the greenness information) and VCI (Vegetation Condition Index) as a way of including crop yield in agricultural droughts (AghaKouchak et al., 2015; Jalili et al., 2014). Another way to account for spatial variability is by hypertunning the parameters of the drought model as done by Ali et al. (2017) and B. Zhang et al. (2023) to achieve more robust prediction results. However, the hypertunning in these studies is limited to prediction module with little physical relevance to spatial and land cover variability in the study area. To our knowledge, there is no previous study that accounts for both climatic and land use variability in large scale areas for drought prediction purposes in the distant future. Therefore, the second knowledge gap we identify in previous studies is lack of capability to capture spatial variability in extensive areas for agricultural droughts prediction and meet the goals of comprehensive drought planning.

To address these two knowledge gaps, the primary goal of this study is to develop a long-term (12 months), large-scale (~700,000 km^2) agricultural drought prediction tool based on remote sensing data. First, we use a modified LSTM specifically designed for long-term prediction (12 months) of climatic variables to address the problem with short forecast horizons. Second, we use precipitation, temperature, and evapotranspiration to include climate variability along with soil moisture and NDVI to account for different land use and cover. We also try to further capture the spatial variability by adding an extra parameter to the prediction module which is the observed return period for each variable. We selected this parameter because it is physically relevant to the spatial and land cover variability and can be used directly in the prediction module to represent previously observed patterns. We improve the model by finetuning the prediction module based on the observed return period for each variable throughout the historical data at different locations. A drought prediction tool specifically designed for a large-scale area can provide the agriculture sector with drought severity maps. This tool can also capture spatial variability and provide various drought propagation patterns that can be analyzed with economic, management, and resource constraints to provide directions for policymaking.

The rest of this paper is organized as follows. Section 2 elucidates the model development, prediction of climatic variables, and calculation of drought indices. Section 3 provides information about the case study area, Texas, US, and the importance of drought prediction there. The model results are outlined in Section 4, and Section 5 compares the performance of the proposed method with other prediction methods in forecasting precipitation values from previous studies. Finally, the conclusions are drawn in Section 6.

2. Methodology

The first step in our method is to preprocess data where climatic variables are retrieved, smoothed, and normalized from remote-sensing sources (Section 2.1). Next, preprocessed data are inputted to a prediction module based on LSTM networks where climatic variables are forecasted for 12 months into the future (Section 2.2). LSTM (Hochreiter & Schmidhuber, 1997) networks are a type of recurrent neural networks capable of learning dependence in sequence prediction problems. The ability to handle vanishing gradients and capture complex temporal patterns makes LSTM a powerful tool for predicting time series especially in hydrology-related applications (Haidar & Verma, 2018; Pathan et al., 2021; Srivastava & Anto, 2022). After this step, predicted variables are combined to compute a drought index which can identify agricultural droughts in the form of drought intensity maps (Section 2.3). Finally, the predicted maps are compared to observed droughts based on reference maps to validate the credibility of our drought prediction tool. In the following sections, each step is explained in detail.

2.1. Data preprocessing

Agricultural drought is a complex phenomenon that requires a combination of hydrometeorological variables to be accurately identified. The most commonly used variables for this task are precipitation, temperature, vegetation condition (usually in the form of NDVI), and soil moisture (Del Pilar Jiménez-Donaire et al., 2020; S. S. Kulkarni et al., 2020a; Sepulcre-Canto et al., 2012). In this study, we use the same four variables to predict agricultural droughts but from remote sensing sources as detailed in Table 1.

Remote sensing data has gained popularity recently due to its global coverage, open access, and grid-based format (Boueshagh and Hasanlou, 2019). Table 1 contains the names of the variables, the satellite image collection, availability period, and spatial and temporal resolutions for each variable. An image collection is a fundamental data structure containing a group of satellite images that share similar properties, such as sensor type, acquisition time, and spatial coverage. An image collection can be easily accessed with a URL and acquire the correspondent dataset. Among the five variables, precipitation is the most important component in identifying agricultural drought. Due to robust representation of spatio-temporal patterns of precipitation (Pradhan et al., 2022), the data used in this study is retrieved from Global Precipitation Measurement (GPM) dataset which is calculated using integrated multi-satellite retrievals for GPM algorithm (EEDC-GPM, 2024). This algorithm is intended to intercalibrate, merge, and interpolate all satellite microwave precipitation estimates, together with microwave-calibrated infrared satellite estimates, precipitation gauge

Table 1
Input variables for prediction module from remote sensing sources.

Variable	Image collection	Period	Spatial resolution	Temporal resolution	Image height	Image width
Precipitation	https://developers.google.com/earth-engine/datasets/catalog/NASA_GPM_L3_IMERG_V06	2001–2022	11132 m	3 h	600	1440
Temperature	https://developers.google.com/earth-engine/datasets/catalog/MODIS_061_MOD11A2	2001–2022	1000 m	8 h	21,600	43,200
NDVI	https://developers.google.com/earth-engine/datasets/catalog/MODIS_061_MOD13A2	2001–2022	1000 m	16 day	16,800	43,200
Soil moisture	https://developers.google.com/earth-engine/datasets/catalog/NASA_GLDAS_V021_NOAH_G025_T3H	2001–2022	27830 m	3 h	600	1440
Evapotranspiration	https://developers.google.com/earth-engine/datasets/catalog/NASA_GLDAS_V021_NOAH_G025_T3H	2001–2022	27830 m	3 h	600	1440

analyses, and potentially other precipitation estimators at higher temporal and spatial scales for the dataset over the entire globe (EEDC-GPM, 2024). Because of higher spatial resolution, temperature and NDVI are both retrieved from Moderate Resolution Imaging Spectroradiometer (MODIS) version 6.1 land data products for different temporal resolutions (EEDC-MODIS, 2024). Soil moisture and evapotranspiration are based on Global Land Data Assimilation System (GLDAS) Version 2.1 validated with a combination of model and observation data from 2000 to present (EEDC-GLDAS, 2024). As done in other machine learning-based prediction models (Latif et al., 2023; Liyew & Melese, 2021), we also use evapotranspiration as an extra feature in the prediction module of precipitation since it directly impacts agricultural management and drought monitoring (Taheri et al., 2022; Khodadadi et al., 2023). Note that evapotranspiration is not included in the calculation of the drought index.

Drought indicators are calculated at monthly scale because periods shorter than a month could make indicators behave erratically (WMO, 2012). Therefore, in this study, all data are averaged to monthly values (from 2001–01 to 2022–12 adding up to 264 months) upon downloading and resampled to a spatial resolution of 27,830 m (0.25 degrees) for consistency. This way, data for each variable becomes available as a grid of cells each with a size of 0.25x0.25 degrees. Additionally, each time series is smoothed by removing outliers using z-score values. The z-score value is a statistical index that shows how distant each point (X) is relative to the mean of data (μ) on a scale of standard deviation (σ) (Eq. (1)). Therefore, a negative (positive) Z-score indicates lower (higher) than mean values.

$$Z = \frac{X - \mu}{\sigma} \tag{1}$$

After calculating z-score values for all data in the time series, outliers are identified by comparing the z-scores to a threshold which is determined experimentally. We tried different values for the threshold and eventually selected threshold $= 5\sigma$because it impacted less than 10 % of the data which meant only the most extreme values were smoothed and the remaining data were left untouched. If the z-score for a value exceeds the threshold, it is considered an outlier. Outliers are then replaced by interpolation using adjacent non-outlier values. Since our model is focused on drought prediction, the smoothing of extreme rainfall values does not mean the removal of extreme drought events. Quite the opposite, this means that the model will be more focused on drought events by paying more attention to the seasonal patterns instead of a handful of extreme rainfall events. Next, we normalize each variable by transforming the values to the range between 0 and 1 to remove the dimension mismatch among variables. Data smoothing and normalization are crucial steps for the prediction module as they can lead to faster convergence and better generalization especially when dealing with variables of different orders and smaller datasets (Alawsi et al., 2022).

2.2. Prediction module

Artificial Neural Networks (ANNs) are a class of machine learning models that can overcome the limitations of the traditional learning algorithms (e.g., logistic regression and support vector machines) with rule-based programming (Lecun et al., 2015). ANNs can be classified into two main categories: FFNNs (feed-forward neural network) and RNNs (recurrent neural network). In FFNNs, there is no connection between the neurons of the same layer; therefore, the information flows in one direction from the input layer to the output layer while passing through hidden layers. On the other hand, RNNs contain connections between neurons within the same hidden layer which enables them to embed historical input information in the learning process. As a result, RNNs are capable of mapping all of the historical input data to the final output and handling temporal dependencies (Hua et al., 2019).

2.2.1. Long Short-Term memory (LSTM)

The key component in the LSTM is the memory block, a recurrently connected subnet that contains functional modules called the memory cell and the gates. The memory cell is responsible for remembering the temporal state of the neural network while the gates control the pattern of information flow. Based on their functionality, these gates are classified as input gate, forget gate, and output gate. The input gate controls the amount of new information flowing into the memory cell; forget gate determines the amount of information that remains in the memory cell at each step; and output gate decides the amount of information used to calculate the output activation of the memory block. This recurrent connection between the memory cell and the gates enables LSTM to predict time series with long-term dependencies (Hua et al., 2019).

In this study, we used layers from TensorFlow (Abadi et al., 2015) and Keras (Chollet & others, 2015) libraries to build our network. TensorFlow is an open-source deep learning framework developed by Google. It provides comprehensive support for building various types of neural networks, including LSTM networks, through its high-level interface called Keras. First, we explain the general training procedure; then, we provide details on the implementation of hyperparameter tunning that led to the selection of model architecture.

Our LSTM network uses m months of data as input to predict 12 months of the target variable as output for each cell individually. As illustrated in Fig. 1, after normalizing, we use a sliding window to reshape 264 months (from 2001–01 to 2022–12) of data into input/output arrays by moving forward one month at each step. LSTM uses m months of historic data from five variables as input ($X = (m, 5)$) to predict the next 12 months of data for the target variable as output ($y = (12,1)$) and measures the accuracy using NSE (Nash–Sutcliffe efficiency (Nash & Sutcliffe, 1970)). NSE ranges from $-\infty$ to 1.0. A value of 1.0 shows perfect agreement between the predictions and the observations, while values closer to 0 indicate poor agreement. Negative values indicate that the mean value of the observations is a better predictor than the model. Due to the heterogenous distribution of climatic variables across the study area, recurring patterns for different cells are not

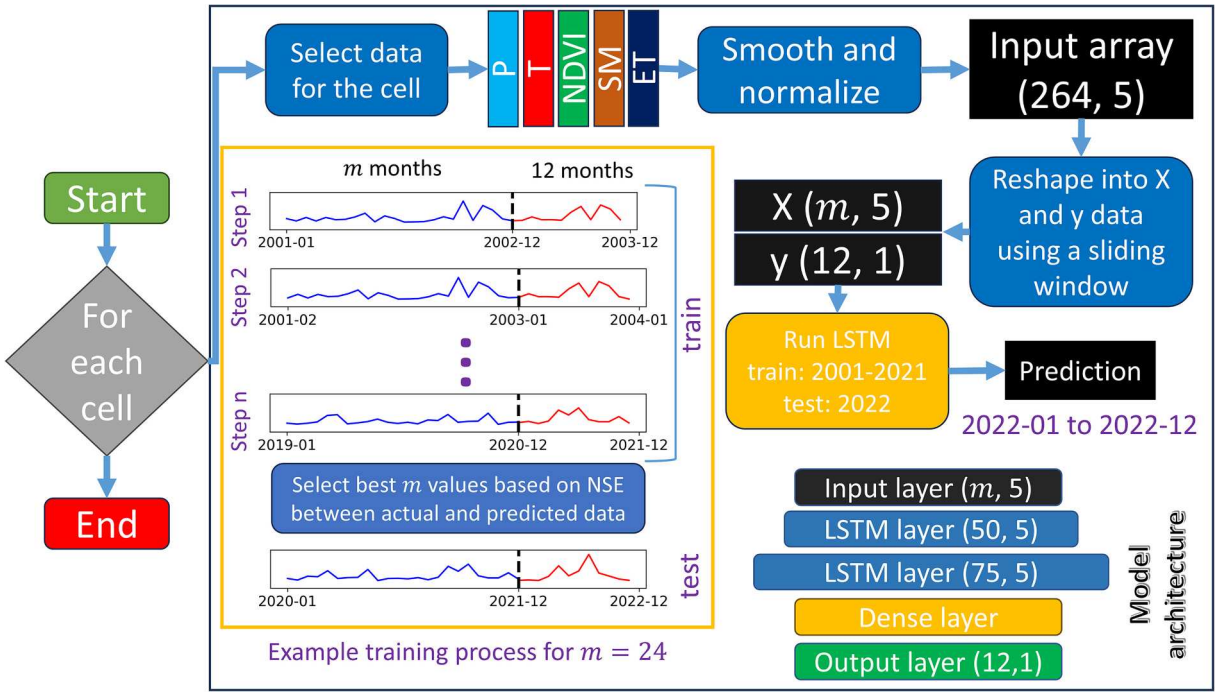

Fig. 1. Prediction module: LSTM runs for each single cell to predict precipitation, temperature, NDVI, and soil moisture from 2022 to 01 to 2022–12. Prediction is finetuned for each cell using different values of *m*.

the same. To capture this variability, we finetune the LSTM by training the model with different values of *m* (12, 24, 36, and 48) separately for each cell. Then, we choose the *m* that yields the highest prediction accuracy on train data (2001–01 to 2021–12) to predict the values for the test data (2022–01 to 2022–12).

Here, we elaborate the process for predicting precipitation for $m = 24$, as an example which is also visualized in Fig. 1. First, LSTM uses 24 months of precipitation, temperature, NDVI, soil moisture, and evapotranspiration from 2001–01 to 2002–12 to predict the precipitation values for 2003–01 to 2003–12 (Step 1); then, moves forward one month for the next step and uses data from five variables from 2001–02 to 2003–01 to predict values from 2003–02 to 2004–01 (Step 2). The training continues until the last step where LSTM uses 24 months of data from 2019–01 to 2020–12 to predict values from 2021–01 to 2021–12 (Step n). Then, the average NSE for all predictions is calculated for the corresponding *m*. After repeating this process for other values of *m*, best value for *m* is determined based on the highest average NSE. Finally, LSTM uses the best value of *m* to predict precipitation from 2022–01 to 2022–12 as test data. This process is repeated for all cells and repeated for the other three target variables (T, NDVI and SM).

We use parameter *m* to account for spatial and temporal heterogeneity in climatic variables in the study area. Parameter *m* determines the number of previous observations needed to predict the next future 12 values; therefore, *m* acts as a physical-temporal hyperparameter that can finetune the LSTM even further for each variable. However, LSTM contains additional parameters that need to be calibrated to achieve the best results. The key parameters include the level of complexity (defined by model architecture which contains formation of layers and number of neurons in each layer), activation function, loss function, number of epochs, and batch size. To determine the best parameters for our model, we run the prediction module for two groups of 3x3 cells in East and West Texas for three different levels of complexity (low, moderate, and high,), three different number of epochs (50, 100, 150), and eight values of batch size (1–8) for all four target variables (precipitation, NDVI, soil moisture, and temperature). In total, we tried 72 combinations of parameters for each variable at each location. Then, evaluated the prediction accuracy by calculating the average NSE for cells in the 3x3 window. Table 2 shows the set of parameters that led to the highest average NSE for each variable at each location.

As shown in Table 2, moderate complexity leads to the highest NSE values for most variables in both East and West Texas. As a result, we selected moderate complexity and epochs=100 as LSTM parameters to run the prediction module for all cells in the study area. This setting is relatively more computationally efficient, generalizes well, and converges faster. Further technical details of hyperparameter tunning for each variable can be found in Tables A1-A5 and Fig. A1-A5 in the Appendix.

2.2.2. *Convolutional neural network (CNN)*

As another machine learning method, we also use Convolutional Neural Networks (CNNs) in our prediction module to compare with LSTM. CNNs can capture spatial dependencies in two-dimensional data which makes them well-suited for tasks like object detection and classification in images (Ahmadi et al., 2023, 2024; Seydi et al., 2024). These networks consist of convolutional, pooling, and fully connected layers that extract features, reduce spatial dimensions and output predictions (Yamashita et al., 2018). 1D-CNNs, a variation of CNNs, are specifically tailored for sequential or time series data, where the input has one-dimensional features. They apply convolutional filters over time

Table 2
Results of hyperparameter tunning for four variables for two groups of 3x3 cells in East and West Texas for 3 different levels of complexity, 3 different number of epochs and 8 values of batch size. NSE_{avg} is the average NSE for cells in the 3x3 window.

Variable	Location	Complexity	Epochs	NSE_{avg}
Precipitation	East	moderate	150	0.0184
Precipitation	West	high	100	0.9050
Temperature	East	moderate	50	0.9399
Temperature	West	moderate	100	0.9595
NDVI	East	moderate	150	0.8904
NDVI	West	high	100	0.9731
Soil moisture	East	moderate	100	0.6956
Soil moisture	West	moderate	150	0.6333

steps to capture local dependencies and temporal patterns effectively (Wibawa et al., 2022). In our study, we utilize 1D-CNNs to predict future values of climatic variables from 2022–01 to 2022–12 using data from 2001–01 to 2021–12 in the training stage. The network architecture along with model parameters are illustrated in Fig. A6 and Table A6 in the Appendix, respectively.

2.2.3. Seasonal autoregressive integrated moving average (SARIMA)

SARIMA is a traditional time series prediction model that integrates seasonal (S), auto-regressive (AR), differencing (I), and moving average (MA) components to model both short-term dependencies and long-term seasonal patterns in time series data (Noor et al., 2022). The inclusion of seasonal components enables SARIMA to handle recurring patterns, the AR component captures the relationship between an observation and a specified number of lagged observations, and the MA component models the residual errors between observations and lagged values. Additionally, the differencing helps to make the data stationary (Dimri et al., 2020). SARIMA has been used widely for the prediction of climatic variables. In general, SARIMA is effective for capturing and forecasting time series data with clear seasonal and cyclical patterns. However, for time series that exhibit highly non-linear or complex behavior, it may underperform (Parasyris et al., 2022). In this study, we use SARIMA to predict future values of climatic variables from 2022–01 to 2022–12 using data from 2001–01 to 2021–12 in the training stage.

2.3. Drought indicators

There are four types of droughts, each affecting different aspects of the environment and society. Meteorological drought refers to a lack of precipitation over a prolonged period and is commonly measured by standardized precipitation index (SPI), which quantifies rainfall deficits over various timescales, first proposed by McKee et al. (1993). A prolonged meteorological drought results in agricultural drought which impacts soil moisture and crop productivity. One of the indicators used to identify agricultural drought is the soil moisture index (SMI) which directly measures the moisture available to plants (Hunt et al., 2009). Hydrological drought is caused by impacts of rainfall deficits on water bodies such as stream flow, reservoir and lake levels and can be measured by surface water supply index (SWSI) (Shafer & Dezman, 1982). Lastly, socio-economic drought links elements of previous drought types with supply and demand of economic goods and can be detected by socio-economic drought information (SEDI) (J. W. Lee et al., 2022). Each indicator provides critical insights into different dimensions of drought, enabling more targeted mitigation strategies.

Agricultural drought occurs as a result of a combination of abnormalities in precipitation, temperature, NDVI, and soil moisture. For this reason, in this study, we use enhanced combined drought index (ECDI) to identify an agricultural drought event based on the results from Enenkel et al. (2016) and Kulkarni et al. (2020b). ECDI is a weighted summation of abnormalities in precipitation, temperature, vegetation condition, and soil moisture ranging from $-\infty$ to $+\infty$ (Eq. (2)). A negative value of ECDI indicates an abnormally dry condition resulting in an agricultural drought with lower values representing more severe droughts. Conversely, a positive value of ECDI refers to wetter than usual conditions and therefore, lower probabilities of drought.

$$ECDI_{y,m} = w_{SPI} \times SPI + w_T \times Z_T + w_{NDVI} \times Z_{NDVI} + w_{SM} \times Z_{SM} \quad (2)$$

Where $ECDI_{y,m}$ is the *ECDI* value for year y and month m, w_X is the corresponding weight of variable X (precipitation, temperature, NDVI, or soil moisture) in identifying an agricultural drought, and Z_X is the z-score value that shows the abnormality in each value of variable X.

In this study, we used Principal Component Analysis (PCA) to determine weights for each variable. PCA is a statistical approach that reduces the dimensionality of a dataset by transforming the original variables into a new set of uncorrelated variables called principal components (Du et al., 2013). In our model, PCA ranks the principal components based on the amount of variance they explain in the data, therefore prioritizing the variables accordingly. Variables that contribute more to the variance of the principal components are considered more important and therefore, are assigned larger weights. For example, for the month January, $w_{SPI} = 0.53$, $w_T = 0.23$, $w_{NDVI} = 0.14$, and $w_{SM} = 0.1$ which means that SPI is a more important variable in the dataset compared to soil moisture. The sum of all weights for the variables by the PCA method adds up to one, ensuring that the relative importance of each variable is captured in a normalized manner (Du et al., 2013). We use SPI as an indicator of abnormality in precipitation because it is widely used as a meteorological drought index to determine the duration and/or severity of a drought event (McKee et al., 1993). SPI values below −1.0 indicate rainfall deficits (drier than normal), while SPI values above 1.0 indicate excess rainfall (wetter than normal) and the values between −1 and 1 correspond to [near] normal conditions (EDO, 2020; WMO, 2012). The lower the SPI, the more severe is the meteorological drought. SPI can be calculated for various time scales, ranging from short-term (e.g., one month) to long-term (e.g., 24 months) since different time scales are useful for assessing different types of droughts. Several studies have used different time scales of SPI (e.g., SPI-1, SPI-2, SPI-3, and SPI-6) to detect agricultural droughts based on the crop type, location and month of drought (Bussay et al., 1999; Cammalleri et al., 2024; Szalai & Szinell, 2000; Y. Zhang et al., 2023). However, in this study, we use SPI-3 (i.e., 3-month SPI) which reportedly has high correlation with agricultural droughts (Irawan et al., 2023; Mohammed et al., 2022). The ECDI ranges and the corresponding drought categories are shown in Table 3. Other elements of ECDI are climatic variables which are already explained in Section 2.1.

Traditional drought prediction tools are based on SPI which only considers the abnormality in precipitation to identify drought events. We also use SPI as one of our variables to detect droughts. In order to validate our model, we compare the drought events between three indicators: SPI-3, ECDI, and USDM (US Drought Monitor) with two purposes. First, evaluate how well previous models (based on SPI) can predict agricultural droughts (SPI-3 vs USDM), and second, assess the impact of additional variables on agricultural drought predictions (ECDI vs USDM). USDM is a weekly map showing the severity of drought events across the US dating back to 2000–01 (USDM, 2023). USDM uses a six-category system, labeled None (Normal or wet conditions), Abnormally Dry or D0, (a precursor to drought, not actually drought), Moderate (D1), Severe (D2), Extreme (D3) and Exceptional (D4) drought. Drought categories show experts' assessments of conditions related to dryness and drought including observations of how much water is available in streams, lakes, and soils compared to usual for the same time of year (USDM, 2023).

However, comparison between USDM and SPI/ECDI values is not straightforward due to two reasons. First, USDM maps are weekly while SPI/ECDI values are monthly. To resolve this issue, weekly USDM maps need to be resampled to monthly scale. In doing so, for each month, the drought category (None, D0, …, D4) that occurs the most is selected as the observed category in that month. If there are two categories with equal number of occurrences in one month, the more severe category is chosen. Second, USDM maps report drought intensity qualitatively using six categories while SPI/ECDI values range from $-\infty$ to $+\infty$ with lower values indicating more severe droughts. We can fix this problem in two

Table 3
ECDI values and the corresponding drought categories based on Kulkarni et al. (2020b).

ECDI values	Drought category	ECDI values	Drought category
2.00 or more	Extremely wet	0 to −0.99	Mildly dry
1.50 to 1.99	Severely wet	−1.00 to −1.49	Moderately dry
1.00 to 1.49	Moderately wet	−1.50 to −1.99	Severely dry
0 to 0.99	Mildly wet	−2.00 or less	Extremely dry

steps. In step 1, a mapping is required to classify continuous values of SPI/ECDI ($-\infty$ to $+\infty$) into six classes to match the categories in USDM (None, D0, D1, D2, D3, D4). For SPI, we use the suggested ranges from USDM manual (Table A7 in the Appendix). Note that the suggested ranges are only used for reference and do not imply that USDM maps are based on SPI values. After classifying SPI values, in step 2, we use a confusion matrix to compare USDM categories with SPI classes. A confusion matrix is a table originally used to evaluate the performance of a binary classification model by tabulating the number of correct and incorrect predictions for each class, however, it can be extended for a multi-class classification model (Kulkarni et al., 2020a). In this study, the rows of the confusion matrix represent the actual classes (USDM), while the columns represent the predicted classes (SPI) (Fig. 2). The confusion matrix is formed by counting the number of occurrences for each possible USDM vs SPI combination for all cells and is calculated for each month separately. For example, in Fig. 2, $TP_{0\text{-}0}$ is the number of cells with drought intensity of D0 from USDM and Class 0 from SPI while $FP_{2\text{-}3}$ is the number of cells where for drought intensity, USDM and SPI reported D2 and Class 3, respectively. As a result, diagonal elements show the number of true predictions (TP) between USDM and SPI while all other elements indicate false predictions (FP).

Naturally, USDM and SPI results are more similar if diagonal elements are larger than all other elements. Based on this, we introduce modified F1-score (Taha & Hanbury, 2015) as an accuracy metric to measure similarity between USDM and SPI values. The F1-score ranges between 0 and 1, where a value of 1 means perfect match between actual and predicted classes and a value of 0 indicates the worst performance. F1-score provides a balanced measure of a model's ability to correctly predict classes while minimizing incorrect predictions and is calculated as follows:

$$F1 = \frac{\sum_c F1_c}{n_c} \quad for\ c\ in\ \{None, D0, D1, D2, D3, D4\} \tag{3}$$

Where F1 is the average of all F1-scores for the number of categories ($n_c = 6$) and $F1_c$ is the F1-score for each row of the table which corresponds to a USDM category (c) (Eq. (4)). Precision is the ratio of true predictions (TP_{c-c}) to the total number of cells where SPI predicted a drought with category c (Eq. (5)) and recall is the ratio of true predictions (TP_{c-c}) to the total number of cells where USDM shows drought with category c (Eq. (6)).

$$F1_c = 2 \times \frac{Precision_c \times Recall_c}{Precision_c + Recall_c} \quad for\ c\ in\ \{None, D0, D1, D2, D3, D4\} \tag{4}$$

$$Precision_c = \frac{TP_{c-c}}{TP_{c-c} + \sum_i FP_{i-c}} \quad for\ i\ in\ \{None, D0, D1, D2, D3, D4\} \tag{5}$$

$$Recall_c = \frac{TP_{c-c}}{TP_{c-c} + \sum_i FP_{c-i}} \quad for\ i\ in\ \{None, Class1, Class2, Class3, Class4\} \tag{6}$$

For ECDI, in step 1, there are no suggested ranges in the literature for mapping continuous ECDI values to USDM categories. We determine this mapping by building a multi-class classification model iteratively for 10,000 randomly generated sets of range values. Each set of range values is created as shown in Table 4, where a, b, c, d, and e are five random numbers based on normal distribution with $\mu = 0.5$ (original interval between categories in ECDI) and $\sigma = 0.1$ (average deviation in lengths of SPI ranges).

At each iteration, we use one set of range values to classify ECDI values into six classes and evaluate the wellness of fit between historical drought events (2001–01 to 2021–12) by ECDI and USDM based on F1-score. The range values that result in the highest F1-score are selected to classify ECDI to USDM categories from 2022–01 to 2022–12. Selected ranges from this process are shown in Table A7 (Appendix).

We also compare prediction results using another metric as quantile loss (Efimov, 2023). Quantile loss provides an indication of the accuracy of predictions, particularly focusing on extreme values of the distribution and ranges from negative infinity to positive infinity. A quantile loss of zero shows perfect predictions at the specified quantile while positive (negative) quantile loss values indicate overestimation (underestimation) of the target values. Quantile loss is calculated for each prediction using the following equation:

$$QL = \begin{cases} q \times (y_{obs} - y_{hat}) if (y_{obs} - y_{hat}) > 0 \\ (q-1) \times (y_{obs} - y_{hat}) if (y_{obs} - y_{hat}) > 0 \end{cases} \tag{7}$$

where QL is the quantile loss, y_{obs} is the observed value, y_{hat} is the predicted value, and q determines which quantile of the distribution is being evaluated. In this study, we used $q = 0.95$ which corresponds to the 95th percentile.

Table 4
Calculation of range values for classification of ECDI values to match drought categories by USDM.

ECDI class	Range	USDM category
Class 4	$(-\infty, -2 + a]$	D4
Class 3	$(-2 + a, -2 + a + b]$	D3
Class 2	$(-2 + a + b, -2 + a + b + c]$	D2
Class 1	$(-2 + a + b + c, -2 + a + b + c + d]$	D1
Class 0	$(-2 + a + b + c + d, -2 + a + b + c + d + e]$	D0
None	$(-2 + a + b + c + d + e, +\infty)$	None

More severe droughts

SPI / USDM	None	Class 0	Class 1	Class 2	Class 3	Class 4
	0.4 or more	0.01 to 0.4	-0.53 to 0.0	-1.08 to -0.54	-1.54 to -1.09	-1.55 or less
None	$TP_{None\text{-}None}$	$FP_{None\text{-}0}$	$FP_{None\text{-}1}$	$FP_{None\text{-}2}$	$FP_{None\text{-}3}$	$FP_{None\text{-}4}$
D0	$FP_{0\text{-}None}$	$TP_{0\text{-}0}$	$FP_{0\text{-}1}$	$FP_{0\text{-}2}$	$FP_{0\text{-}3}$	$FP_{0\text{-}4}$
D1	$FP_{1\text{-}None}$	$FP_{1\text{-}0}$	$TP_{1\text{-}1}$	$FP_{1\text{-}2}$	$FP_{1\text{-}3}$	$FP_{1\text{-}4}$
D2	$FP_{2\text{-}None}$	$FP_{2\text{-}0}$	$FP_{2\text{-}1}$	$TP_{2\text{-}2}$	$FP_{2\text{-}3}$	$FP_{2\text{-}4}$
D3	$FP_{3\text{-}None}$	$FP_{3\text{-}0}$	$FP_{3\text{-}1}$	$FP_{3\text{-}2}$	$TP_{3\text{-}3}$	$FP_{3\text{-}4}$
D4	$FP_{4\text{-}None}$	$FP_{4\text{-}0}$	$FP_{4\text{-}1}$	$FP_{4\text{-}2}$	$FP_{4\text{-}3}$	$TP_{4\text{-}4}$

More severe droughts

Fig. 2. Confusion matrix for comparing USDM with SPI values between all cells for each month. SPI classes are based on suggested ranges from USDM manual. For each cell, if both USDM and SPI point to the same drought category, we get a true prediction (TP); otherwise, we get a false prediction (FP).

3. Study area

We use the State of Texas, US, as our study area where agriculture is one of the most important sectors. Texas leads the nation in number of farms and ranches, with 248,416 farms and ranches covering 127 million acres that resulted in a $24.9 billion revenue from agricultural products in 2017 (TDOA, 2023). Unfortunately, Texas has a long history of droughts with the worst one being the seven-year drought of record in the 1950s with a total loss of $36 billion. Since then, Texas has faced several droughts, including the drought of 2011 that was unprecedented in its intensity with a total loss of $11.1–15.5 billion (Nielsen-Gammon, 2012). Drought is a growing concern in Texas as the year 2022 was the 11th driest year in the past 128 years and the worst drought since 2011 (Donald & Grubbs, 2022). Therefore, there is an urge to address the gaps and improve previous drought prediction tools to reduce the impacts and prevent catastrophic droughts in future.

As a starting point, we try to identify spatial and temporal patterns in climatic variables by finding groups of cells that exhibit similarities in historic time series. Precipitation, temperature, NDVI, and soil moisture are the main inputs of the prediction module as the core of each drought prediction tool. Identifying patterns in these variables can provide valuable insights to improve the prediction module and therefore the drought prediction tool. Texas has 10 distinct climatic zones based on the distribution of annual average temperature and precipitation (TWDB, 2012). The average annual precipitation increases almost uniformly from 25 cm in the west to 140 cm in the southeast (Wong et al., 2015), which explains the dense population of southeast Texas compared to western parts. The wet season in Texas is mainly from March to May and sometimes from September to October (USCD, 2024), where the wettest and driest areas receive approximately 150 and 30 rainy days, respectively (Ghebreyesus & Sharif, 2020). Fig. 3 shows the recurring intervals (i.e., return period) in precipitation values for all cells where the x-axis is the return period in precipitation and y-axis is the cell number on the grid. To calculate these intervals, first we converted time series values into frequency domain using Fast Fourier Transform (FFT) with an interval of one month; then inverted the frequency values to obtain periods as recurring intervals. As demonstrated, there is a clear recurring pattern in 12 months for all cells (continuous vertical line at x = 12). This line is clearer and more consistent for cells 0–1500 which mainly belong to West and Central Texas (Fig. 3a). On the other hand, for cells 1500–2256 that belong to East Texas, there are other lines at each row (Fig. 3b). This indicates that there is often more than one recurring pattern for each cell and the clear annual period is distorted by other recurring intervals because of complex precipitation patterns in this area (Lyons, 1990). This heterogeneous distribution of precipitation is partly due to El Niño and La Niña which impact rainfall through altering atmospheric circulation and influencing the jet streams (Mauget & Upchurch, 1999; Slade & Chow, 2011) that mainly affect East Texas and result in different recurring patterns for precipitation in the State of Texas.

The uneven precipitation patterns also affect other climatic variables and lead to complex patterns over time for West versus East Texas as shown in Fig. 4. As an example, we selected cells 5, 33, 101, and 192 from West Texas and cells 1773, 1850, 1999, and 2027 from East Texas (Fig. 4a) and plotted time series for precipitation, temperature, NDVI, and soil moisture from 2001 to 2022. Neighbor cells show similar patterns and therefore are not visualized. As illustrated in Fig. 4b, there are clearer annually recurring patterns in all four variables from 2001 to 2022 for cells in West Texas. On the other hand, for cells in East Texas, patterns for precipitation and soil moisture are much more complex (Fig. 4c) and do not follow any clear recurring interval. These different patterns are proof that a prediction model with only one period as the recurring interval for all cells cannot be both accurate and generalize well for a study area as large as the State of Texas with heterogenous climatic patterns.

4. Results

4.1. Prediction accuracy of climatic variables

Prediction module is the core of our drought prediction model. Since the prediction is implemented on each cell, prediction accuracy results are displayed as maps. Fig. 5 shows prediction accuracy maps based on NSE values between observations and predictions for 2022–01 to 2022–12 for all four variables. As illustrated, prediction accuracy for each variable follows a different spatial pattern. First, we explain why accuracy values for predicting precipitation are higher for West Texas compared to East Texas (Fig. 5a). As a machine learning model, LSTM needs to learn from historical data and be trained to predict future values accurately which happens successfully in most parts of the study area with higher accuracy values in West and Central Texas. Since there are clear recurring patterns for precipitation in West and Central Texas both in train and test data, LSTM is trained more efficiently and can achieve higher accuracy values in this region.

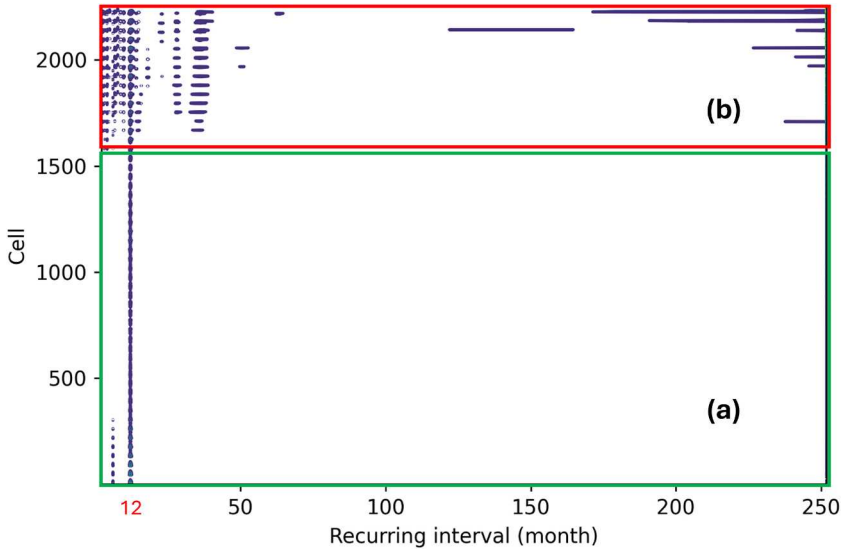

Fig. 3. Recurring intervals for all cells based on Fast Fourier Transform (FFT); a) Cells 0–1500 (West and Central Texas) show clear annual recurring patterns; b) Cells 1500–2256 (East Texas) exhibit various recurring intervals due to more complex precipitation patterns.

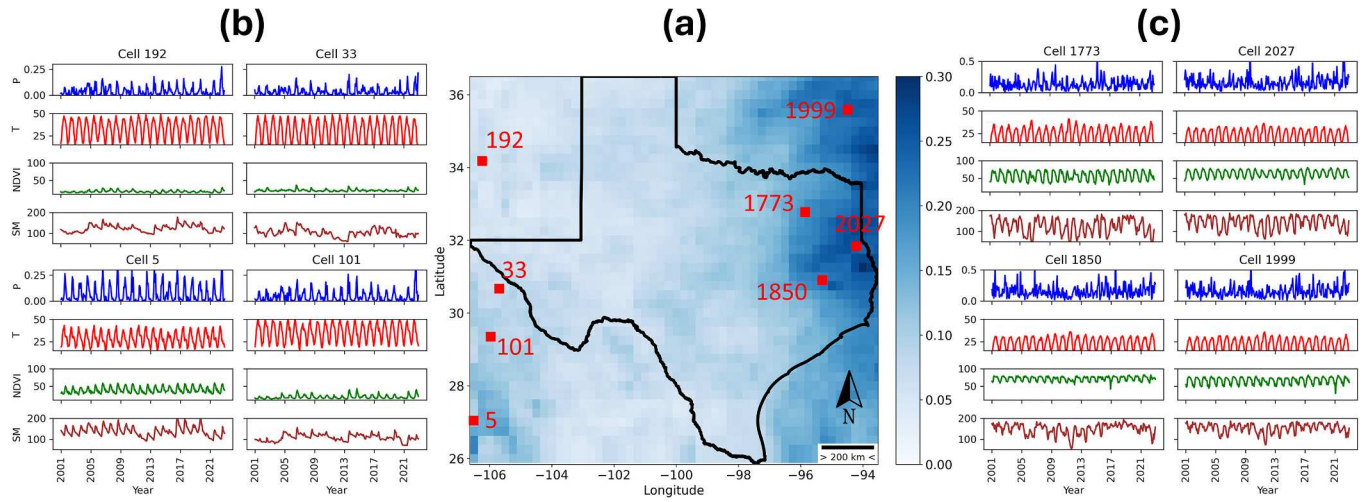

Fig. 4. a) average monthly precipitation (mm/hr) for 2022; b & c) time series of climatic variables including precipitation (P), temperature (T), NDVI, and soil moisture (SM), from 2001 to 2022 for West (cells 5, 33, 101, and 192) vs East (cells 1773, 1850, 1999, and 2027) Texas. In contrast to East Texas, West Texas shows clearer recurring patterns for all four variables.

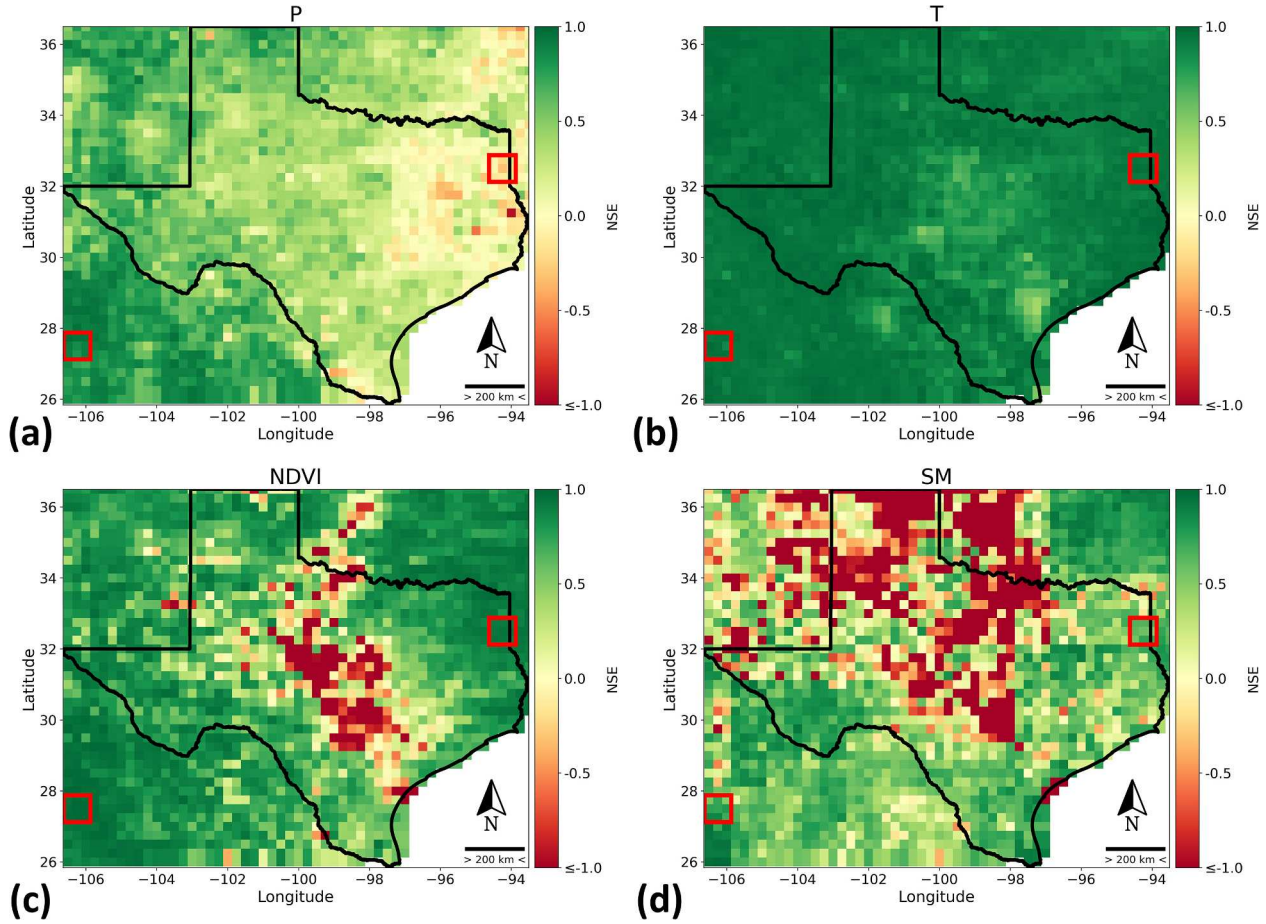

Fig. 5. Prediction accuracy maps for a) precipitation (P), b) temperature (T), c) NDVI, and d) soil moisture (SM) based on NSE values. Temperature and soil moisture show the highest and lowest average NSE values, respectively. This is due to the spatial distribution of precipitation and temperature over the State of Texas.

To further explain this difference, we show time series of normalized precipitation at two distant locations in the study area with different values of prediction accuracy. To avoid one single cell outlier, we selected a 3x3 window of cells (cells 5, 6, 7, 48, 49, 50, 91, 92, and 93) to represent West Texas (Fig. 6a). As illustrated, precipitation shows clear annually repeating patterns for cells in West Texas that only differ in peak values. LSTM can learn such patterns during the train period and output accurate prediction for test data. On the other hand, for cells in East Texas (cells 1941, 1942, 1943, 1984, 1985, 1986, 2027, 2028, and 2029), patterns are much more complex such that there is often more than one wet season throughout the year in addition to no clear repeating cycles (Fig. 6b). This difference is also illustrated in the Fast

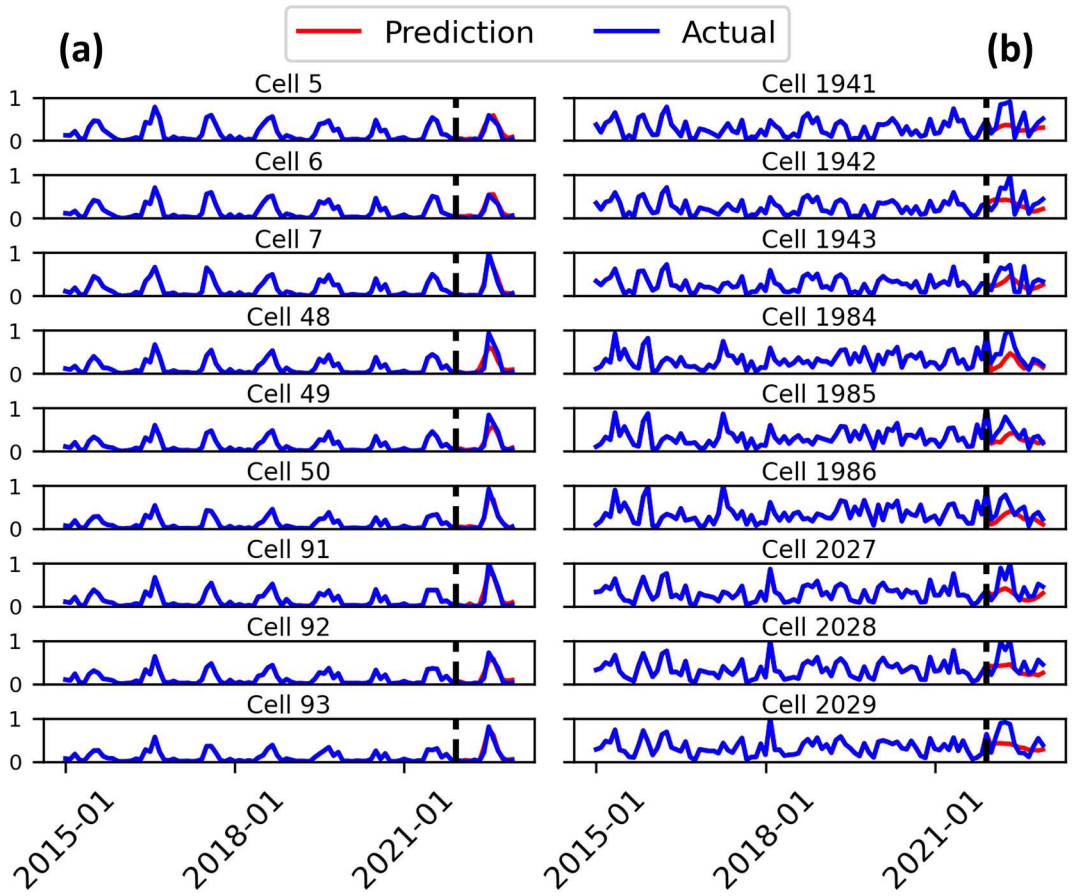

Fig. 6. Time series for precipitation at two distant locations for a 3x3 window of 9 cells to represent a) West and b) East Texas as drawn in Fig. 5. Cells in West Texas show similar precipitation patterns in both train and test data which enables LSTM to learn these patterns and yield accurate predictions. On the other hand, LSTM does not output accurate predictions for cells in East Texas since there are no clear patterns in historic data.

Fourier Transform results of Fig. 3 where cells 1500–2256 (located in East Texas) show multiple complex recurring intervals while cells 0–1500 (located in West and Central Texas) show much clearer patterns with annual return periods. In the absence of such clear patterns for cells in East Texas, based on the definition of loss function within it, LSTM tries to predict the most frequently observed average behavior in recent years which might not always lead to an accurate prediction. As a result, prediction of precipitation in East Texas is less accurate compared to West Texas.

In contrast to precipitation, temperature values exhibit very similar patterns both in West (Fig. 7a) and East (Fig. 7b) Texas. Temperature patterns are more stable throughout the years and show much lower variance compared to precipitation, NDVI, and soil moisture. This might be because precipitation can have a larger impact on NDVI and soil moisture compared to temperature. These patterns repeat during both the train and test periods. As a result, LSTM can be trained efficiently and learn the patterns to predict test data with high accuracy in both locations. In other words, for temperature, there are consistently clear patterns all over Texas which enables LSTM to yield accurate predictions for temperature at all cells.

Prediction accuracy patterns for soil moisture and NDVI are similar to each other but different from precipitation. One of the factors that impact soil moisture and therefore NDVI is human activities that include agricultural practices (e.g., irrigation and groundwater withdrawal), overgrazing, deforestation, and urbanization (Wei et al., 2022). These activities impact soil moisture and eventually vegetation cover which in turn can reduce water infiltration and lower soil moisture levels even further (Huang et al., 2021; Yang et al., 2023). The areas with low prediction accuracy for soil moisture on the map are mainly located in regions where the most grazing (USDA, 2024) and groundwater withdrawal (Holt, 2024) happens along with cultivation of different crops such as wheat, corn, and cotton (USDA, 2020). The combination of these factors results in complex patterns for soil moisture and therefore lower prediction accuracy. In general, LSTM yields accurate predictions only in cells that exhibit a recurring pattern throughout both train and test data. Time series for NDVI and SM are provided in Fig. A7 in the Appendix.

4.2. Comparison between predicted ECDI and actual SPI-3

Using predictions from all four variables, ECDI values are calculated by taking weights from PCA which ranks the most important variables in the dataset. Fig. 8 visualizes predicted ECDI vs SPI-3 values obtained from actual observations from 2022–01 to 2022–12. As shown, ECDI and SPI-3 show similar spatial patterns but different intensities for drought events in consecutive months (Fig. 8a and 8b). Based on the definition of ECDI, the severity of an agricultural drought is the result of not only lower precipitation but also extreme temperatures and abnormally low NDVI and soil moisture which can further enhance drought severity and cause different intensities compared to SPI-3 which is only affected by precipitation. These conditions can subsequently result in stability of drought severity in consecutive months in ECDI maps compared to SPI-3. Other studies have pointed out this stability in drought conditions for other combined drought indicators in comparison with SPI (Bernard et al., 2013; Cammalleri et al., 2021; Faiz et al., 2022; J. Li et al., 2024). As visualized in Fig. 8c for 2022–03 and 2022–04 for SPI-3, the drought condition for the two regions outlined changes from Extremely Dry to Severely Wet in only one month. This may be the result of an increase in

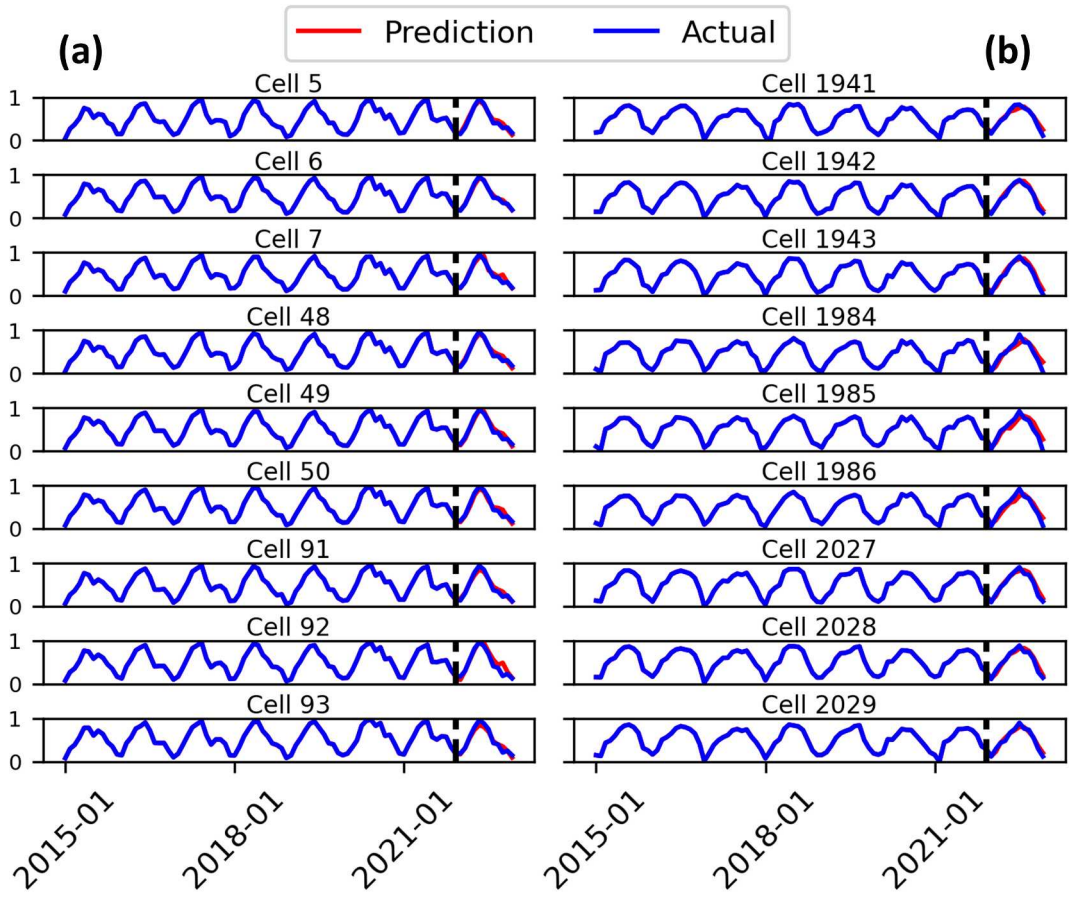

Fig. 7. Time series for temperature at two distant locations for a 3x3 window of 9 cells to represent a) West and b) East Texas. All cells contain recurring patterns which enables LSTM to learn these patterns and output accurate results at both locations.

precipitation which, based on the definition of SPI, ends the drought period for the regions of interest. On the other hand, as shown in Fig. 8d the same two regions on the ECDI maps show gradual change in drought severity. Although precipitation increases in these regions, it takes longer for other variables such as NDVI and soil moisture to recover from the drought impacts which causes the longer duration of an agricultural drought versus a drought based on SPI. Several studies have pointed out this delay in recovering from drought impacts despite the resumption of more normal precipitation after drought ends (Peterson et al., 2021; Schreiner-McGraw & Ajami, 2021; L. Zhang et al., 2024). This makes ECDI a more suitable indicator for identifying a more consistency and stability agricultural. Another example is outlined between 2022–08 and 2022–09 from SPI maps (Fig. 8e) where the drought condition goes from Mildly Wet to Extremely Dry in just one month while changes in ECDI maps (Fig. 8f) are much less intensive. Results for other months in 2022 are portrayed in Fig. A8 in the Appendix.

4.3. Comparison between classified ECDI/SPI and USDM

In this section, we compare our results to another drought index, USDM as reference. We selected USDM since it is widely used by several organizations to determine drought conditions or for financial purposes (USDM, 2023). Fig. 9 shows drought intensity maps for classified ECDI/SPI-3 and USDM in three months in 2022 that represent three different stages of the drought event in 2022. First, we compare the drought extent by visually inspecting maps. As visualized in Fig. 9a, the majority of Texas experienced extensive droughts in 2022–01 which is captured by all three indicators. Additionally, according to USDM, the worst drought happened in 2022–06 (Fig. 9b); however, SPI-3 reports Normal or Wet condition for this month indicating no droughts at all. In contrast to SPI-3, ECDI does exhibit droughts in 2022–06 for western and central parts of Texas but with different intensity compared to USDM (Abnormally Dry vs Extreme Drought). Similarly, in Fig. 9c, both USDM and ECDI show extensive droughts in 2022–12 while SPI-3 indicates no droughts in most parts of the study area. This is because agricultural droughts are caused by a combination of factors including lack of precipitation, high temperature, low crop yield (low NDVI) and soil moisture deficit. ECDI can detect agricultural droughts since it contains additional variables for capturing such factors. However, SPI only relies on precipitation and cannot do this. Results for other months in 2022 are included in Fig. A9 in the Appendix.

In order to compare drought intensity between the indices, we use F1-score values from confusion matrices as explained in the methodology section. F1-scores for ECDI/SPI vs USDM are included in Fig. 10. In general, F1-scores are relatively low (< 0.4) which indicates low similarity between ECDI/SPI and USDM. The reason for this lies in the classification of ECDI/SPI values to match corresponding drought categories in USDM. ECDI/SPI are computation-based indices while USDM is a qualitative human-made map; therefore, converting a quantitative value into a quality-based index comes with an inevitable bias which depends on the month and the region of interest. More specifically, F1-score values are higher in months 1–3 and 10–12 and lower in months 4–9, resulting in a parabolic shape. This is because in months 4–9 most crops are irrigation-based which means more human interference and therefore, addition of qualitative criteria in drought identification by USDM. These criteria include characteristics of different crops, irrigation patterns, people's subjective beliefs about the severity of drought events, etc. Such human-dependent criteria are not considered in ECDI/SPI which causes less similarity between ECDI/SPI and USDM droughts and therefore, lower F1-scores in these months. On the other hand, for

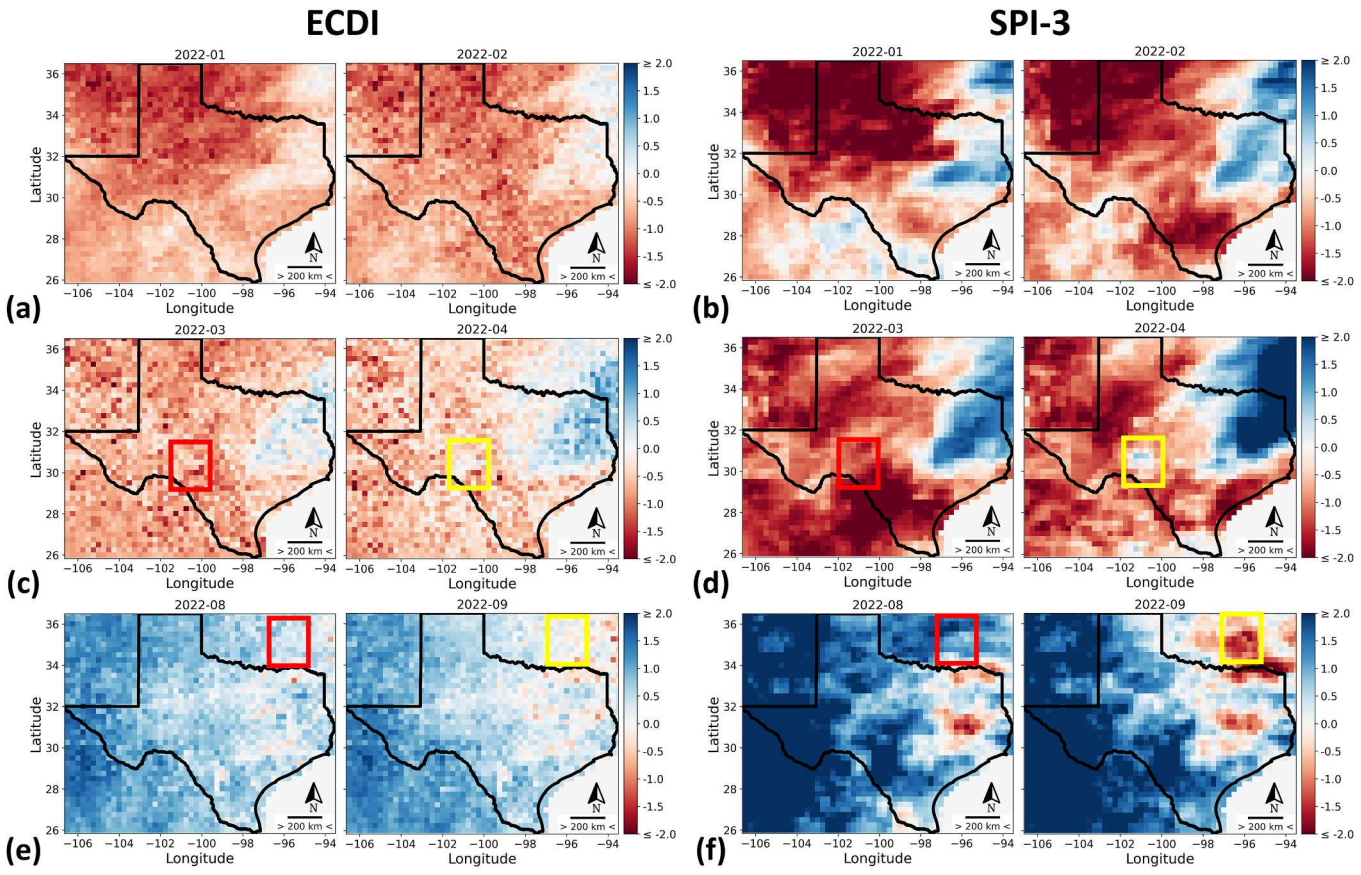

Fig. 8. Comparing ECDI (a, c, e) with SPI-3 (b, d, f) for six months in 2022; both ECDI and SPI-3 exhibit similar spatial patterns but with different intensities for drought events. Due to additional variables in the definition of ECDI, it can capture agricultural droughts with higher temporal consistency.

months 1–3 and 10–12, most vegetation cover is related to rainfed crops or pastures. This means less human activity and therefore more similarity between ECDI/SPI and USDM. With that in mind, F1-scores for ECDI vs USDM are higher than the corresponding values for SPI vs USDM in all months especially in the early and later stages of drought (months 1–4 and 9–12).

After comparing results in case of drought extent and severity, we can observe more similarity and correspondence between ECDI and USDM compared to SPI-3 and USDM. USDM is just another drought index and since human subjectivity is included in the production of the USDM maps (Hatami Bahman Beiglou et al., 2021), it might not be accurate at all times. However, the US drought agency uses USDM to trigger disaster declarations and eligibility for low-interest loans (USDM, 2023). Based on results provided above, predicted droughts by ECDI are similar to actual droughts by USDM in case of extent and intensity at different stages of droughts. Since USDM is a real-time index, it can only be used for drought monitoring and not prediction. In this case, predicted droughts from ECDI can inform the authorities about future droughts, especially in the early stages of a drought event.

5. Discussion

5.1. Comparison of different prediction methods

Prediction module is the core of every drought prediction tool. In this section, while comparing model structure uncertainty (i.e., different results due to different computational methods) is not the main focus on this paper, we show the results of precipitation prediction for three of the most common prediction methods to shed light on this topic. We test two other methods for this purpose: 1D-CNN and SARIMA.

Fig. 11 shows the results of three methods for prediction of precipitation values. Here, we adjusted the NSE range to focus on positive values instead of negative ones to measure the precisions of models in drought-prone regions. According to different studies, worst droughts in Texas occur in western and central regions (Lowry, 1959; McGovern, 2023; SCCSC, 2018). As demonstrated, LSTM has higher prediction accuracy in these regions followed by 1D-CNN and SARIMA. On the other hand, SARIMA outperforms LSTM and 1D-CNN in predicting precipitation values for cells in East Texas where drought is not considered a problem due to abundance of precipitation and access to groundwater. These cells contain very complex patterns with no clear recurring cycles. Neither SARIMA nor LSTM can capture the extreme precipitation values in this region; however, SARIMA performs better at capturing the general pattern because it uses moving average components from historical data to predict future values. In order to analyze results from LSTM and SARIMA in more depth, we used quantile loss which focuses on the prediction accuracy of extreme values with a quantile value of 0.95. Absolute quantile loss values for comparing observations vs. predictions for LSTM and SARIMA models are equal to 0.021 and 0.054. To further examine this difference, Fig. 12 shows actual precipitations, predictions from LSTM, and predictions from SARIMA for two groups of cells as representative of West and East Texas. As demonstrated in Fig. 12a, SARIMA underestimates precipitation values in 7 out of 9 cells in West Texas. respectively. This shows that LSTM performs better than SARIMA at predicting extreme values in West Texas, where there are clear recurring patterns for precipitation and drought is considered a critical issue. Furthermore, we expanded the comparison between models by running the prediction models for NDVI as an additional variable. We selected NDVI because it contains both simple and complex patterns all over Texas and is also an important variable in determining agricultural drought conditions. Results of this step are provided in Fig. A10 in the Appendix. We also compared LSTM and SARIMA in case of

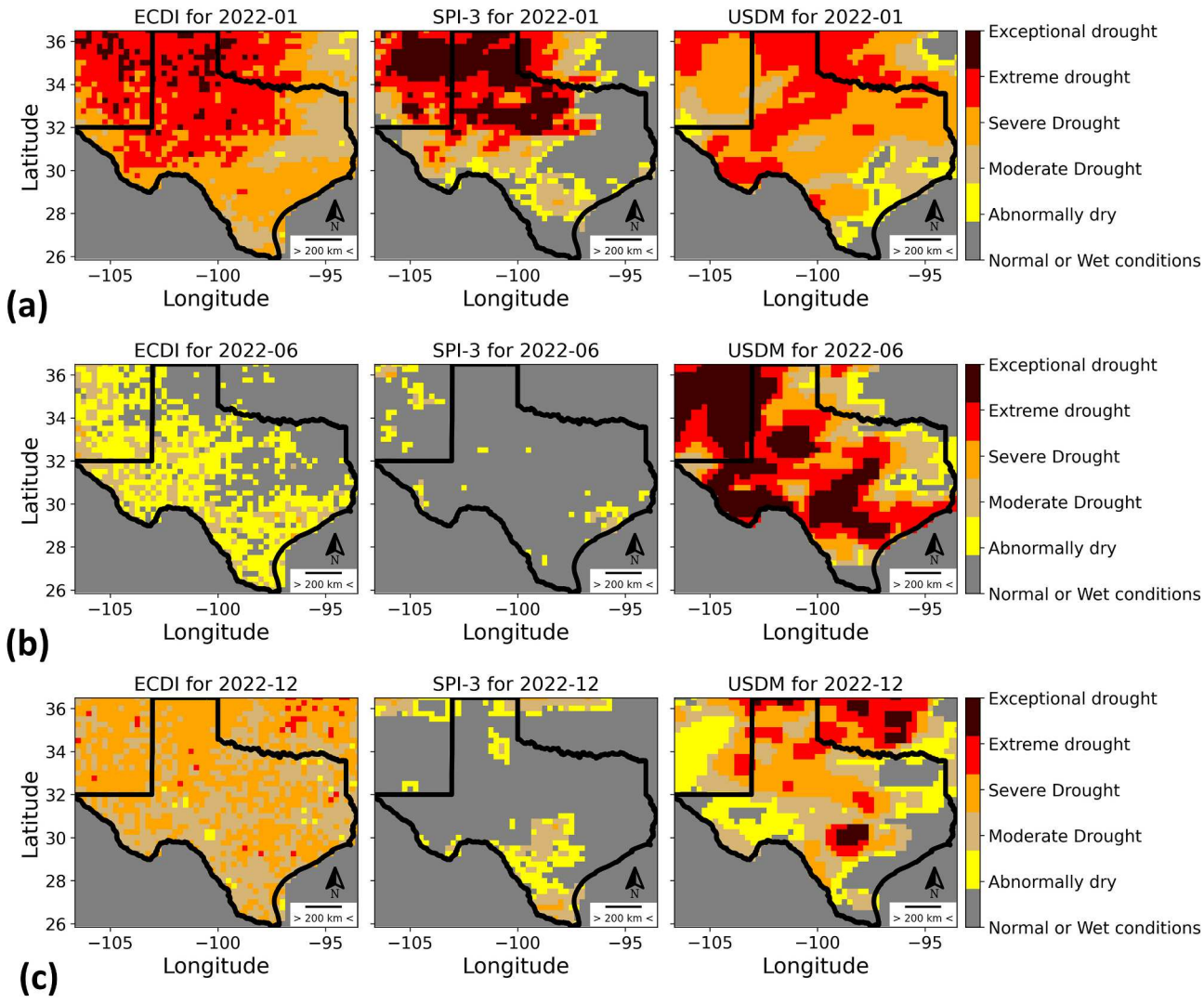

Fig. 9. Drought intensity maps based on classified ECDI/SPI vs USDM in 2022 for a) January, b) June, and c) December. ECDI is more capable of capturing the spatial extent of droughts as indicated by USDM.

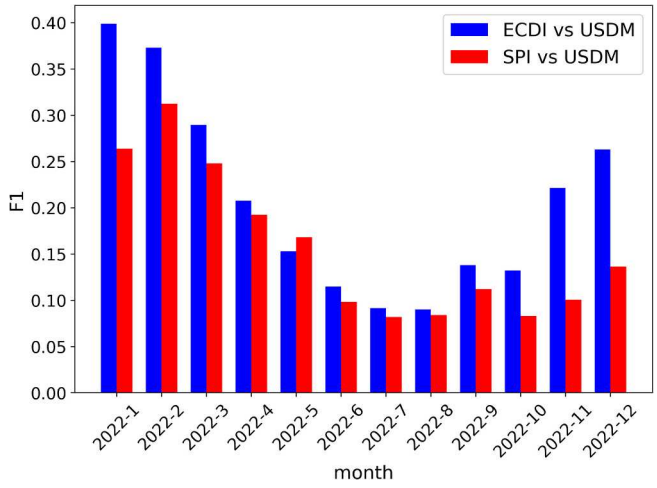

Fig. 10. F1-scores from confusion matrices for comparing drought intensity of ECDI/SPI to USDM. ECDI shows higher F1-scores in all months especially in the early and later stages of drought.

computational time by running each model on a desktop Dell Precision Tower 3620 with an Intel Corei7-7700 K CPU and 64 GBs of RAM. SARIMA predicts future values by optimizing several parameters known as model configuration. This is done by running the model for every possible combination of these parameters which can be extremely time consuming especially if run on a cell by cell basis. In our case, SARIMA completed predictions in nearly 158 h while LSTM was able to do so in 84 h.

5.2. *Limitations and future works*

The current drought prediction tool we developed has several limitations. First, we resampled all variables to a spatial resolution of 0.25 degrees which equals the resolution of remote sensing-based soil moisture. Although this reduces the computational load of the model, a higher resolution is preferred for more accurate planning. To overcome this, we can enhance the spatial resolution of remote sensing data used in this study. This has been done for other datasets in recent studies; for example, Imanpour et al. (2023) used two numerical methods, regression and ANN to downscale the soil moisture data from Soil Moisture Active Passive (SMAP) dataset. In another study, Brown & Long (2022) employed the Scatterometer Image Reconstruction algorithm in its radiometer form to enhance the resolution of the radiometer brightness

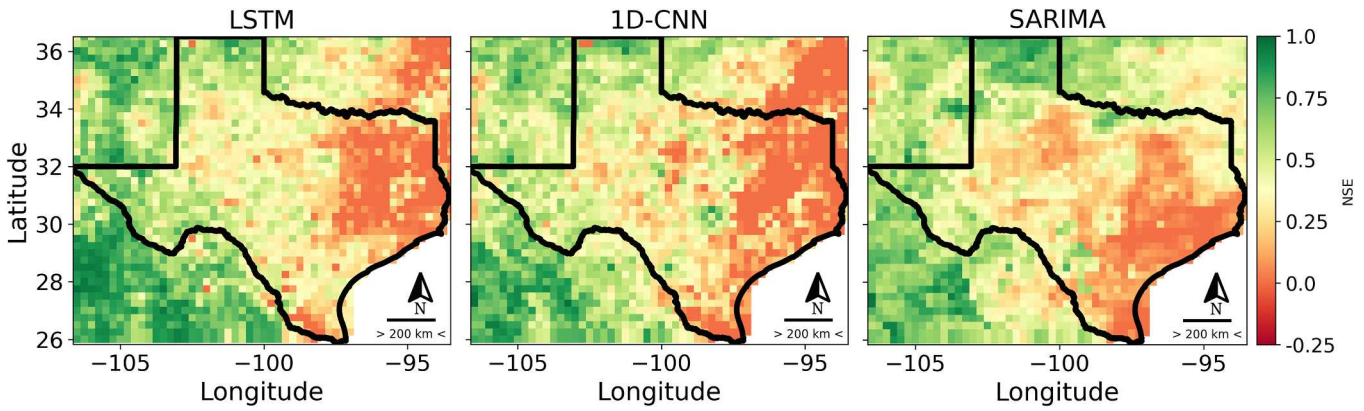

Fig. 11. Prediction accuracy results for precipitation based on adjusted NSE score. LSTM performs the best in West and Central Texas where droughts have the highest intensity.

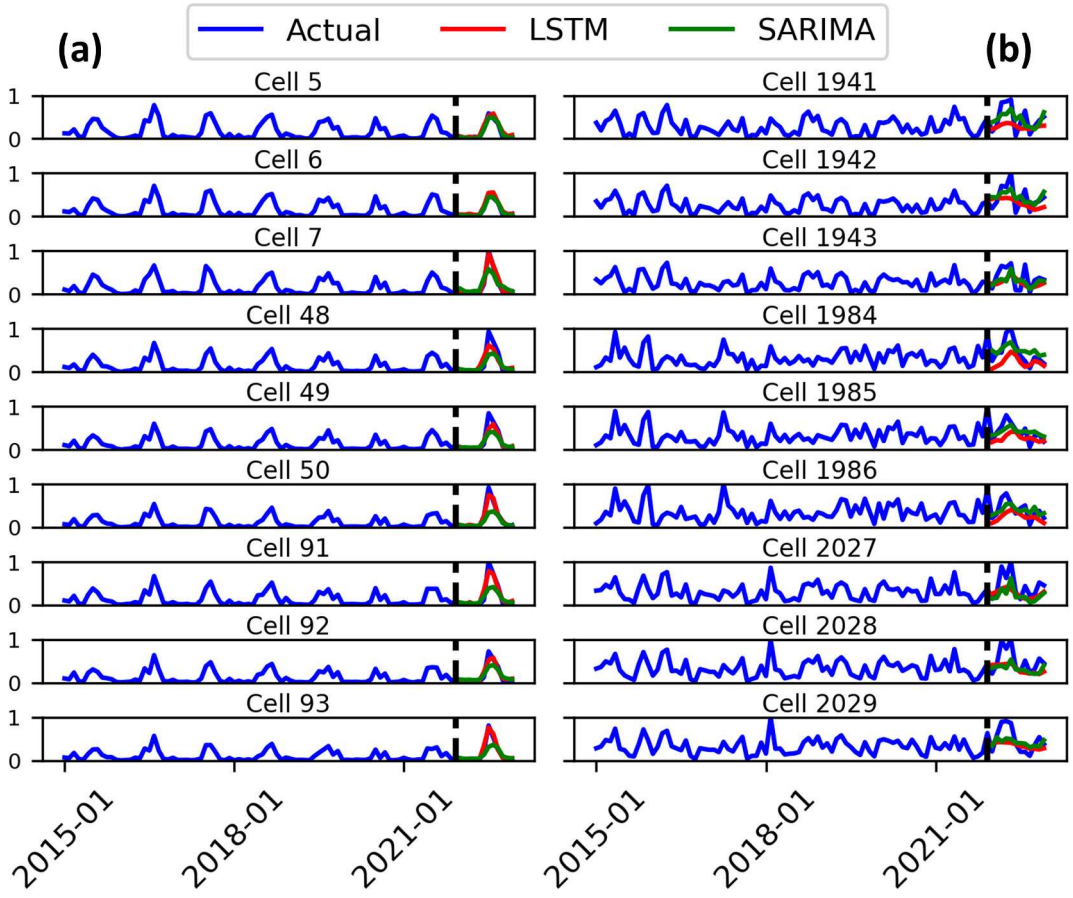

Fig. 12. Comparison of actual precipitations with predictions by LSTM and SARIMA for a) West and b) East Texas. LSTM performs better in West Texas where droughts are worse while SARIMA captures the general trend with higher accuracy in East Texas where droughts are less intensive.

temperature measurements and therefore improve the resolution of soil moisture from SMAP dataset. Implementation of such methods is location-dependent and requires ground-based observations for validation. Second, the architecture for LSTM was selected through trial and error and we did not optimize each parameter in the model separately since it was very time consuming. To improve this, we can fine-tune the general model by optimizing several parameters instead of only one (m = number of previous months used to predict next 12 months) using Bayesian optimization or random search. Third, while we aimed to quantitatively compare the results between station-based and remote sensing data, we encountered challenges related to the availability of key datasets such as NDVI and soil moisture in our study area from ground-based datasets. This limitation prevented us from conducting a direct comparison between ground-based observations and remote sensing data. However, we recognize the potential for future investigations to address this gap by leveraging alternative ECDIs for remote sensing and ground-based data or by exploring additional sources of data for vegetation and soil moisture. These efforts could enhance our understanding of drought dynamics and improve the reliability of our analyses.

Another way to improve the current study is by including other factors that contribute to spatial variability such as resource constraints

(e.g., water), farmers' income and crop types for each cell similar to the studies done by Chen et al. (2014b), Toscano-Pulido et al. (2024), and Ghaffari et al. (2022). This way, we can develop maps of drought vulnerability in addition to drought severity to identify the most vulnerable regions under various drought events. This can result in a more comprehensive and accurate planning for a large-scale area like the State of Texas. Prediction accuracy maps can identify the regions where prediction of future variables becomes more challenging for LSTM. It is possible to develop a local small-scale drought prediction tool using LSTM as prediction method for every distinct region with similar patterns in historical data. This might improve the prediction accuracy but with two major challenges. First, the results of such models will be local and not necessarily applicable to a large-scale area due to consistency issues. Second, development of such models requires an accurate classification model to separate cells with similar patterns into different groups for each variable. This can increase the computational burden of the model significantly without guaranteeing an improvement in prediction accuracy.

6. Conclusion

Drought prediction tools can forecast future droughts to mitigate the impacts on crop production and assist the agriculture sector in planning for minimizing the effects. With the increasing observation of more frequent and severe droughts all over the world in recent years, the need for improved models for drought planning and management in the distant future is getting urgent. In this study, we developed a long-term (12 months) drought prediction tool based on LSTM using only remote sensing data to address the issue with short forecast horizon. Additionally, we extended model application to extensive areas by capturing spatial variability of different factors in the prediction module. The new drought prediction tool uses enhanced combine drought index (ECDI) to determine the severity of drought events which is a combination of anomalies in precipitation, temperature, NDVI, and soil moisture.

Our results showed that droughts predicted based on ECDI show similar spatial patterns but different intensities compared to droughts predicted based on standardized precipitation index (SPI). Drought events change more gradually between consecutive months since temperature, NDVI, and soil moisture can further impact the severity of droughts in ECDI results. This implies ECDI can be a more appropriate index to capture agricultural droughts with more stability. We also compared drought prediction results based on ECDI/SPI with human-made reference drought maps: USDM. ECDI demonstrate a stronger capability (than SPI) to capture the spatial extent of USDM's drought results with some discrepancies in the drought intensity. This is because the process of converting continuous values of ECDI into qualitative categories of USDM is not definite and may lead to discordance in intensity which is due to their different nature. To compare drought intensity between the three indicators in different months, we used F1-scores which showed that ECDI results are more similar to USDM compared to SPI-3. Additionally, we compared the prediction accuracy results for precipitation between LSTM, 1D-CNN, and SARIMA. LSTM performed better than SARIMA in areas with worse drought conditions (West and Central Texas) while SARIMA was able to capture the general pattern in areas with less severe droughts (East Texas) with higher accuracy.

The methodology introduced in this study can be applied globally with available remote sensing data. The longer prediction horizon and large-scale application of this model can provide the authorities with a longer lead time to prepare for and mitigate the impacts of agricultural droughts for policymaking purposes. Finally, we suggest three possible directions to improve upon our current model: use finer resolution data, optimize the prediction module more extensively, and build a hybrid drought prediction tool using both ground-based and remote sensing data to add to the reliability of our results.

CRediT authorship contribution statement

Ali Ghaffari: Writing – review & editing, Writing – original draft, Visualization, Validation, Software, Project administration, Methodology, Investigation, Funding acquisition, Formal analysis, Data curation, Conceptualization. **Shrouq Abuismail:** Writing – review & editing, Methodology. **Y.C. Ethan Yang:** Supervision, Methodology, Formal analysis, Conceptualization, Writing – review & editing. **Maryam Rahnemoonfar:** Writing – review & editing.

Declaration of competing interest

The authors declare that they have no known competing financial interests or personal relationships that could have appeared to influence the work reported in this paper.

Acknowledgment

The work described in this paper was supported by the US National Science Foundation (NSF): CBET #1941727 and US Department of Energy (DOE): DE-SC0025413. We also want to thank comments from editors, reviewers and Dr. Aparna Bharati (Department of Computer Science at Lehigh University) who helped us improve the quality of the manuscript.

Appendix A. Supplementary data

Supplementary data to this article can be found online at https://doi.org/10.1016/j.jhydrol.2025.133316.

Data availability

The data used is publicly available.

References

Abadi, M., Agarwal, A., Barham, P., Brevdo, E., Chen, Z., Citro, C., Corrado, G. S., Davis, A., Dean, J., Devin, M., Ghemawat, S., Goodfellow, I., Harp, A., Irving, G., Isard, M., Jozefowicz, R., Jia, Y., Kaiser, L., Kudlur, M., … Zheng, X. (2015). TensorFlow: Large-scale machine learning on heterogeneous systems. Software available from tensorflow. org.

AghaKouchak, A., Farahmand, A., Melton, F.S., Teixeira, J., Anderson, M.C., Wardlow, B. D., Hain, C.R., 2015. Remote sensing of drought: Progress, challenges and opportunities. Rev. Geophys. 53 (2), 452–480. https://doi.org/10.1002/2014RG000456.

Agrawal, S., Barrington, L., Bromberg, C., Burge, J., Gazen, C., & Hickey, J. (2019). Machine Learning for Precipitation Nowcasting from Radar Images. https://arxiv.org/abs/1912.12132v1.

Ahmadi, M., Gholizadeh Lonbar, A., Nouri, M., Sharifzadeh Javidi, A., Tarlani Beris, A., Sharifi, A., Salimi-Tarazouj, A., 2024. Supervised multi-regional segmentation machine learning architecture for digital twin applications in coastal regions. J. Coast. Conserv. 28 (2), 1–15. https://doi.org/10.1007/S11852-024-01038-1/METRICS.

Ahmadi, M., Lonbar, A. G., Sharifi, A., Beris, A. T., Nouri, M., & Javidi, A. S. (2023). Application of Segment Anything Model for Civil Infrastructure Defect Assessment. https://arxiv.org/abs/2304.12600v1.

Akbari Asanjan, A., Yang, T., Hsu, K., Sorooshian, S., Lin, J., Peng, Q., 2018. Short-Term Precipitation Forecast Based on the PERSIANN System and LSTM Recurrent Neural Networks. J. Geophys. Res. Atmos. 123 (22), 12543–12563. https://doi.org/10.1029/2018JD028375.

Alawsi, M. A., Zubaidi, S. L., Al-Bdairi, N. S. S., Al-Ansari, N., & Hashim, K. (2022). Drought Forecasting: A Review and Assessment of the Hybrid Techniques and Data Pre-Processing. Hydrology 2022, Vol. 9, Page 115, 9(7), 115. doi: 10.3390/HYDROLOGY9070115.

Ali, Z., Hussain, I., Faisal, M., Nazir, H.M., Hussain, T., Shad, M.Y., Mohamd Shoukry, A., Hussain Gani, S., 2017. Forecasting Drought Using Multilayer Perceptron Artificial Neural Network Model. Adv. Meteorol. 2017. https://doi.org/10.1155/2017/5681308.

Bernard, B., Vincent, K., Frank, M., Anthony, E., 2013. Comparison of extreme weather events and streamflow from drought indices and a hydrological model in River Malaba, Eastern Uganda. Int. J. Environ. Stud. 70 (6), 940–951. https://doi.org/10.1080/00207233.2013.862463.

Boueshagh, M., Hasanlou, M., 2019. ESTIMATING WATER LEVEL IN THE URMIA LAKE USING SATELLITE DATA: A MACHINE LEARNING APPROACH. In: The International Archives of the Photogrammetry, Remote Sensing and Spatial

Information Sciences, Vol. XLII-4/W18. Copernicus GmbH, pp. 219–226. https://doi.org/10.5194/isprs-archives-xlii-4-w18-219-2019.
Bowles, T.M., Mooshammer, M., Socolar, Y., Calderón, F., Cavigelli, M.A., Culman, S.W., Deen, W., Drury, C.F., Garcia y Garcia, A., Gaudin, A. C. M., Harkcom, W. S., Lehman, R. M., Osborne, S. L., Robertson, G. P., Salerno, J., Schmer, M. R., Strock, J., & Grandy, A. S., 2020. Long-Term Evidence Shows that Crop-Rotation Diversification Increases Agricultural Resilience to Adverse Growing Conditions in North America. One Earth 2 (3), 284–293. https://doi.org/10.1016/J.ONEEAR.2020.02.007.
Brown, J.P., Long, D.G., 2022. Resolution Enhancement of SMAP Passive Soil Moisture Estimates. Remote Sens. (Basel) 14 (7), 1761. https://doi.org/10.3390/rs14071761.
Bussay, A., Szinell, C., Szentimery, T., 1999. Investigation and Measurements of Droughts in Hungary. Hungarian Meteorological Service.
Cammalleri, C., Arias-Munõz, C., Barbosa, P., De Jager, A., Magni, D., Masante, D., Mazzeschi, M., McCormick, N., Naumann, G., Spinoni, J., 2021. A revision of the Combined Drought Indicator (CDI) used in the European Drought Observatory (EDO). Nat. Hazards Earth Syst. Sci. 21 (2), 481–495. https://doi.org/10.5194/NHESS-21-481-2021.
Cammalleri, C., McCormick, N., Spinoni, J., Nielsen-Gammon, J.W., 2024. An Analysis of the Lagged Relationship between Anomalies of Precipitation and Soil Moisture and Its Potential Role in Agricultural Drought Early Warning. J. Appl. Meteorol. Climatol. 63 (2), 339–350. https://doi.org/10.1175/JAMC-D-23-0077.1.
Chang, W.S., Lin, Y.T., 2019. The effect of lead-time on supply chain resilience performance. Asia Pac. Manag. Rev. 24 (4), 298–309. https://doi.org/10.1016/J.APMRV.2018.10.004.
Chen, H., Wang, J., Huang, J., 2014. Policy support, social capital, and farmers' adaptation to drought in China. Glob. Environ. Chang. 24 (1), 193–202. https://doi.org/10.1016/J.GLOENVCHA.2013.11.010.
Chollet, F., & others. (2015). Keras.
Damberg, L., AghaKouchak, A., 2014. Global trends and patterns of drought from space. Theor. Appl. Climatol. 117 (3–4), 441–448. https://doi.org/10.1007/S00704-013-1019-5/FIGURES/3.
Del Pilar Jiménez-Donaire, M., Tarquis, A., Vicente Giráldez, J., 2020. Evaluation of a combined drought indicator and its potential for agricultural drought prediction in southern Spain. Natural Hazards and Earth System Sciences 20 (1), 21–33. https://doi.org/10.5194/NHESS-20-21-2020.
Dimri, T., Ahmad, S., Sharif, M., 2020. Time series analysis of climate variables using seasonal ARIMA approach. J. Earth Syst. Sci. 129 (1), 1–16. https://doi.org/10.1007/S12040-020-01408-X/TABLES/7.
Donald, J., Grubbs, S., 2022. December). Drought in Texas, FiscalNotes https://comptroller.texas.gov/economy/fiscal-notes/2022/dec/drought.php.
Du, L., Tian, Q., Yu, T., Meng, Q., Jancso, T., Udvardy, P., Huang, Y., 2013. A comprehensive drought monitoring method integrating MODIS and TRMM data. Int. J. Appl. Earth Obs. Geoinf. 23 (1), 245–253. https://doi.org/10.1016/J.JAG.2012.09.010.
EDO. (2020). Standardized Precipitation Index (SPI). https://drought.emergency.copernicus.eu/data/factsheets/factsheet_spi.pdf.
EEDC-GLDAS. (2024). GLDAS-2.1: Global Land Data Assimilation System | Earth Engine Data Catalog | Google for Developers. https://developers.google.com/earth-engine/datasets/catalog/NASA_GLDAS_V021_NOAH_G025_T3H.
EEDC-GPM. (2024). GPM: Global Precipitation Measurement (GPM) v6 | Earth Engine Data Catalog | Google for Developers. https://developers.google.com/earth-engine/datasets/catalog/NASA_GPM_L3_IMERG_V06.
EEDC-MODIS. (2024). MODIS: Moderate Resolution Imaging Spectroradiometer (MODIS) version 6.1 | Earth Engine Data Catalog | Google for Developers. https://developers.google.com/earth-engine/datasets/catalog/MODIS_061_MOD11A2.
Efimov, V. (2023). Quantile Loss & Quantile Regression | Towards Data Science. https://towardsdatascience.com/quantile-loss-and-quantile-regression-b0689c13f54d.
Enenkel, M., Steiner, C., Mistelbauer, T., Dorigo, W., Wagner, W., See, L., Atzberger, C., Schneider, S., & Rogenhofer, E. (2016). A Combined Satellite-Derived Drought Indicator to Support Humanitarian Aid Organizations. Remote Sensing 2016, Vol. 8, Page 340, 8(4), 340. doi: 10.3390/RS8040340.
Faiz, M.A., Zhang, Y., Zhang, X., Ma, N., Aryal, S.K., Ha, T.T.V., Baig, F., Naz, F., 2022. A composite drought index developed for detecting large-scale drought characteristics. J. Hydrol. 605, 127308. https://doi.org/10.1016/J.JHYDROL.2021.127308.
Gamboa-Villafruela, C. J., Fernández-Alvarez, J. C., Márquez-Mijares, M., Pérez-Alarcón, A., & Batista-Leyva, A. J. (2021). Convolutional LSTM Architecture for Precipitation Nowcasting Using Satellite Data. Environmental Sciences Proceedings 2021, Vol. 8, Page 33, 8(1), 33. doi: 10.3390/ECAS2021-10340.
Ghaffari, A., Nasseri, M., Pasebani Someeh, A., 2022. Assessing the economic effects of drought using Positive Mathematical Planning model under climate change scenarios. Heliyon 8 (12), e11941. https://doi.org/10.1016/j.heliyon.2022.e11941.
Ghebreyesus, D., & Sharif, H. O. (2020). Spatio-Temporal Analysis of Precipitation Frequency in Texas Using High-Resolution Radar Products. Water 2020, Vol. 12, Page 1378, 12(5), 1378. doi: 10.3390/W12051378.
Haidar, A., Verma, B., 2018. Monthly Rainfall Forecasting Using One-Dimensional Deep Convolutional Neural Network. IEEE Access 6, 69053–69063. https://doi.org/10.1109/ACCESS.2018.2880044.
Beiglou, H.B., P., Luo, L., Tan, P. N., & Pei, L., 2021. Automated Analysis of the US Drought Monitor Maps With Machine Learning and Multiple Drought Indicators. Front. Big Data 4. https://doi.org/10.3389/FDATA.2021.750536.
Hochreiter, S., Schmidhuber, J., 1997. Long Short-Term Memory. Neural Computation 9 (8), 1735–1780. https://doi.org/10.1162/NECO.1997.9.8.1735.
Holt, I., 2024. July 3). Texas groundwater depth map, Banks Environmental Data https://www.banksinfo.com/blog/comprehensive-groundwater-depth-map-texas/.
Hua, Y., Zhao, Z., Li, R., Chen, X., Liu, Z., Zhang, H., 2019. Deep Learning with Long Short-Term Memory for Time Series Prediction. IEEE Commun. Mag. 57 (6), 114–119. https://doi.org/10.1109/MCOM.2019.1800155.
Huang, C., Yang, Q., Huang, W., 2021. Analysis of the Spatial and Temporal Changes of NDVI and Its Driving Factors in the Wei and Jing River Basins. Int. J. Environ. Res. Public Health 18 (22), 11863. https://doi.org/10.3390/IJERPH182211863.
Hunt, E.D., Hubbard, K.G., Wilhite, D.A., Arkebauer, T.J., Dutcher, A.L., 2009. The development and evaluation of a soil moisture index. Int. J. Climatol. 29 (5), 747–759. https://doi.org/10.1002/JOC.1749.
Imanpour, F., Dehghani, M., Yazdi, M., 2023. Improving SMAP soil moisture spatial resolution in different climatic conditions using remote sensing data. Environ. Monit. Assess. 195 (12). https://doi.org/10.1007/S10661-023-12107-7.
Irawan, A.N.R., Komori, D., Hendrawan, V.S.A., 2023. Correlation analysis of agricultural drought risk on wet farming crop and meteorological drought index in the tropical-humid region. Theor. Appl. Climatol. 153 (1–2), 227–240. https://doi.org/10.1007/S00704-023-04461-W/FIGURES/12.
Jalili, M., Gharibshah, J., Ghavami, S.M., Beheshtifar, M., Farshi, R., 2014. Nationwide prediction of drought conditions in Iran based on remote sensing data. IEEE Trans. Comput. 63 (1), 90–101. https://doi.org/10.1109/TC.2013.118.
Kabbilawsh, P., Kumar, D.S., Chithra, N.R., 2022. Forecasting long-term monthly precipitation using SARIMA models. J. Earth Syst. Sci. 131 (3), 1–20. https://doi.org/10.1007/S12040-022-01927-9/FIGURES/7.
Khodadadi, M., Maleki Roozbahani, T., Taheri, M., Ganji, F., Nasseri, M., 2023. The effect of embedding actual evapotranspiration uncertainty in water balance model: coupling of interval-based hydrologic model and METRIC method. Acta Geophysica 72 (3), 1985–2007. https://doi.org/10.1007/s11600-023-01112-6.
Kulkarni, A., Chong, D., Batarseh, F.A., 2020a. Foundations of data imbalance and solutions for a data democracy. Data Democracy: at the Nexus of Artificial Intelligence, Software Development, and Knowledge Engineering 83–106. https://doi.org/10.1016/B978-0-12-818366-3.00005-8.
Kulkarni, S. S., Wardlow, B. D., Bayissa, Y. A., Tadesse, T., Svoboda, M. D., & Gedam, S. S. (2020a). Developing a Remote Sensing-Based Combined Drought Indicator Approach for Agricultural Drought Monitoring over Marathwada, India. Remote Sensing 2020, Vol. 12, Page 2091, 12(13), 2091. doi: 10.3390/RS12132091.
Kulkarni, S.S., Wardlow, B.D., Bayissa, Y.A., Tadesse, T., Svoboda, M.D., Gedam, S.S., 2020c. Developing a remote sensing-based combined drought indicator approach for agricultural drought monitoring over Marathwada, India. Remote Sens. (Basel) 12 (13). https://doi.org/10.3390/RS12132091.
Kumar, P., Shah, S. F., Uqaili, M. A., Kumar, L., & Zafar, R. F. (2021). Forecasting of Drought: A Case Study of Water-Stressed Region of Pakistan. Atmosphere 2021, Vol. 12, Page 1248, 12(10), 1248. doi: 10.3390/ATMOS12101248.
Latif, S.D., Hazrin, A.B., N., Hoon Koo, C., Lin Ng, J., Chaplot, B., Feng Huang, Y., El-Shafie, A., & Najah Ahmed, A., 2023. Assessing rainfall prediction models: Exploring the advantages of machine learning and remote sensing approaches. Alex. Eng. J. 82, 16–25. https://doi.org/10.1016/J.AEJ.2023.09.060.
Lecun, Y., Bengio, Y., & Hinton, G. (2015). Deep learning. Nature 2015 521:7553, 521 (7553), 436–444. doi: 10.1038/nature14539.
Lee, J.W., Hong, E.M., Jang, W.J., Kim, S.J., 2022. Assessment of socio-economic drought information using drought-related Internet news data (Part A: Socio-economic drought data construct and evaluation socio-economic drought information). Int. J. Disaster Risk Reduct. 75, 102961. https://doi.org/10.1016/J.IJDRR.2022.102961.
Lee, T., Ouarda, T.B.M.J., 2010. Long-term prediction of precipitation and hydrologic extremes with nonstationary oscillation processes. J. Geophys. Res. Atmos. 115 (D13), 13107. https://doi.org/10.1029/2009JD012801.
Li, J., Li, Y., Yin, L., Zhao, Q., 2024a. A novel composite drought index combining precipitation, temperature and evapotranspiration used for drought monitoring in the Huang-Huai-Hai Plain. Agric Water Manag 291, 108626. https://doi.org/10.1016/J.AGWAT.2023.108626.
Li, Y., Huang, Y., Li, Y., Zhang, H., Fan, J., Deng, Q., & Wang, X. (2024). Spatiotemporal heterogeneity in meteorological and hydrological drought patterns and propagations influenced by climatic variability, LULC change, and human regulations. Scientific Reports 2024 14:1, 14(1), 1–18. doi: 10.1038/s41598-024-56526-z.
Liyew, C.M., Melese, H.A., 2021. Machine learning techniques to predict daily rainfall amount. Journal of Big Data 8 (1), 1–11. https://doi.org/10.1186/S40537-021-00545-4/TABLES/3.
Lowry, R. L. (1959). A Study of Droughts in Texas.
Lu, J., Li, G., Cheng, C., -, al, R Moustafa, S. S., Khodairy -, S. S., Chen, P., Niu, A., Liu, D., Jiang, W., & Ma, B., 2018. Time Series Forecasting of Temperatures using SARIMA: An Example from Nanjing. IOP Conf. Ser.: Mater. Sci. Eng. 394 (5), 052024. https://doi.org/10.1088/1757-899X/394/5/052024.
Luo, C., Li, X., Ye, Y., 2021. PFST-LSTM: A SpatioTemporal LSTM Model with Pseudoflow Prediction for Precipitation Nowcasting. IEEE J. Sel. Top. Appl. Earth Obs. Remote Sens. 14, 843–857. https://doi.org/10.1109/JSTARS.2020.3040648.
Lyons, S.W., 1990. Spatial and Temporal Variability of Monthly Precipitation in Texas. Mon. Weather Rev. 118 (12), 2634–2648. https://doi.org/10.1175/1520-0493(1990)118<2634:SATVOM>2.0.CO;2.
Malik, A., Kumar, A., 2020. Meteorological drought prediction using heuristic approaches based on effective drought index: a case study in Uttarakhand. Arab. J. Geosci. 13 (6), 1–17. https://doi.org/10.1007/S12517-020-5239-6/FIGURES/7.
Mardian, J. (2022). The role of spatial scale in drought monitoring and early warning systems: a review. Doi: 10.1139/Er-2021-0102, 30(3), 438–459. doi: 10.1139/ER-2021-0102.
Mauget, S.A., Upchurch, D.R., 1999. El Niño and La Niña Related Climate and Agricultural Impacts over the Great Plains and Midwest. J. Prod. Agric. 12 (2), 203–215. https://doi.org/10.2134/JPA1999.0203.

McGovern, M. (2023, March 5). Where is Texas' drought the worst? https://www.ketk.com/news/texas/where-is-texas-drought-the-worst/.
McKee, T. B., Doesken, N. J., & Kleist, J. (1993). The Relationship of Drought Frequency and Duration to Time Scales. 8th Conference on Applied Climatology, Anaheim, 17-22 January 1993, 179–184.
Meydani, A., Dehghanipour, A., Schoups, G., Tajrishy, M., 2022. Daily reservoir inflow forecasting using weather forecast downscaling and rainfall-runoff modeling: Application to Urmia Lake basin. Iran Journal of Hydrology: Regional Studies 44, 101228. https://doi.org/10.1016/J.EJRH.2022.101228.
Meydani, A., Dehghanipour, A., Tajrishy, M., 2021. Development of a Daily Rainfall-Runoff Model to Simulate the Bukan Reservoir Inflow and Quantify the Effects of Severe Historical Drought Using WEAP Model and MultiObjective Calibration. Iran-Water Resources Research 17 (3), 149–164. https://doi.org/10.1007/978-3-540-75941-6_9.
Mishra, A.K., Singh, V.P., 2011. Drought modeling – A review. J. Hydrol. 403 (1–2), 157–175. https://doi.org/10.1016/J.JHYDROL.2011.03.049.
Mohammed, S., Alsafadi, K., Enaruvbe, G. O., Bashir, B., Elbeltagi, A., Széles, A., Alsalman, A., & Harsanyi, E. (2022). Assessing the impacts of agricultural drought (SPI/SPEI) on maize and wheat yields across Hungary. Scientific Reports 2022 12:1, 12(1), 1–19. doi: 10.1038/s41598-022-12799-w.
Nash, J.E., Sutcliffe, J.V., 1970. River flow forecasting through conceptual models part I — A discussion of principles. J. Hydrol. 10 (3), 282–290. https://doi.org/10.1016/0022-1694(70)90255-6.
National Weather Service. (2023, October 25). National Weather Service. NOAA's National Weather Service. https://www.weather.gov/safety/drought-types#:~:text=Agricultural%20Drought%20refers%20to%20the,reservoir%20levels%20needed%20for%20irrigation.
Nguyen, V.H., Li, Q.F., Nguyen, L.B., 2017. Drought forecasting using ANFIS- a case study in drought prone area of Vietnam. Paddy Water Environ, 15 (3), 605–616. https://doi.org/10.1007/S10333-017-0579-X/FIGURES/7.
Nielsen-Gammon, J.W., 2012. The 2011 Texas Drought. Texas Water Journal 3 (1), 59–95. https://doi.org/10.21423/TWJ.V3I1.6463.
Noor, T. H., Almars, A. M., Alwateer, M., Almaliki, M., Gad, I., & Atlam, E. S. (2022). SARIMA: A Seasonal Autoregressive Integrated Moving Average Model for Crime Analysis in Saudi Arabia. Electronics 2022, Vol. 11, Page 3986, 11(23), 3986. doi: 10.3390/ELECTRONICS11233986.
Parasyris, A., Alexandrakis, G., Kozyrakis, G. V., Spanoudaki, K., & Kampanis, N. A. (2022). Predicting Meteorological Variables on Local Level with SARIMA, LSTM and Hybrid Techniques. Atmosphere 2022, Vol. 13, Page 878, 13(6), 878. doi: 10.3390/ATMOS13060878.
Parker, B.A., Lisonbee, J., Ossowski, E., Prendeville, H.R., Todey, D., 2023. Drought Assessment in a Changing Climate: Priority Actions and Research Needs. https://doi.org/10.25923/5zm3-6x83.
Pathan, M. S., Jain, M., Lee, Y. H., Skaif, T. Al, & Dev, S. (2021). Efficient Forecasting of Precipitation Using LSTM. Progress in Electromagnetics Research Symposium, 2021-November, 2312–2316. doi: 10.1109/PIERS53385.2021.9694772.
Peterson, T.J., Saft, M., Peel, M.C., John, A., 2021. Watersheds may not recover from drought. Science 372 (6543), 745–749. https://doi.org/10.1126/SCIENCE.ABD5085/SUPPL_FILE/ABD5085S2.MP4.
Pradhan, R.K., Markonis, Y., Vargas Godoy, M.R., Villalba-Pradas, A., Andreadis, K.M., Nikolopoulos, E.I., Papalexiou, S.M., Rahim, A., Tapiador, F.J., Hanel, M., 2022. Review of GPM IMERG performance: A global perspective. Remote Sens. Environ. 268, 112754. https://doi.org/10.1016/J.RSE.2021.112754.
Qiu, M., Zhao, P., Zhang, K., Huang, J., Shi, X., Wang, X., Chu, W., 2017. A short-term rainfall prediction model using multi-task convolutional neural networks. In: Proceedings - IEEE International Conference on Data Mining. https://doi.org/10.1109/ICDM.2017.49.
Sadeghi, M., Asanjan, A.A., Faridzad, M., Nguyen, P.H.U., Hsu, K., Sorooshian, S., Braithwaite, D.A.N., 2019. PERSIANN-CNN: Precipitation Estimation from Remotely Sensed Information Using Artificial Neural Networks–Convolutional Neural Networks. J. Hydrometeorol. 20 (12), 2273–2289. https://doi.org/10.1175/JHM-D-19-0110.1.
Safari, S., Sharghi, S., Kerachian, R., Noory, H., 2023. A market-based mechanism for long-term groundwater management using remotely sensed data. J. Environ. Manage. 332, 117409. https://doi.org/10.1016/J.JENVMAN.2023.117409.
SCCSC. (2018). Drought History for Texas' 10 Regions.
Schreiner-McGraw, A.P., Ajami, H., 2021. Delayed response of groundwater to multi-year meteorological droughts in the absence of anthropogenic management. J. Hydrol. 603, 126917. https://doi.org/10.1016/J.JHYDROL.2021.126917.
Schwantes, A.M., Parolari, A.J., Swenson, J.J., Johnson, D.M., Domec, J.-C., Jackson, R. B., Pelak, N.F., Porporato, A., 2018. Accounting for landscape heterogeneity improves spatial predictions of tree vulnerability to drought. Civil and Environmental Engineering Faculty Research and Publications 226.
Sepulcre-Canto, G., Horion, S., Singleton, A., Carrao, H., Vogt, J., 2012. Development of a Combined Drought Indicator to detect agricultural drought in Europe. Nat. Hazards Earth Syst. Sci. 12 (11), 3519–3531. https://doi.org/10.5194/NHESS-12-3519-2012.
Seydi, S. T., Boueshagh, M., Namjoo, F., Minouei, S. M., Nikraftar, Z., & Amani, M. (2024). A Hyperspectral Change Detection (HCD-Net) Framework Based on Double Stream Convolutional Neural Networks and an Attention Module. Remote Sensing 2024, Vol. 16, Page 827, 16(5), 827. doi: 10.3390/RS16050827.
Shafer, B.A., Dezman, L.E., 1982. Development of a Surface Water Supply Index (SWSI) to Assess the Severity of Drought Conditions in Snowpack Runoff Areas. In: Proceedings of the Western Snow Conference, pp. 164–175.
Shi, X., Gao, Z., Lausen, L., Wang, H., Yeung, D.-Y., Wong, W., & WOO, W. (2017). Deep Learning for Precipitation Nowcasting: A Benchmark and A New Model. In I. Guyon, U. Von Luxburg, S. Bengio, H. Wallach, R. Fergus, S. Vishwanathan, & R. Garnett (Eds.), Advances in Neural Information Processing Systems (Vol. 30). Curran Associates, Inc. https://proceedings.neurips.cc/paper_files/paper/2017/file/a6db4ed04f1621a119799fd3d7545d3d-Paper.pdf.
Slade, R.M., Chow, T.E., 2011. Statistical relations of precipitation and stream runoff for El Niño and La Niña periods. Texas Hill Country. Texas Water Journal 2 (1), 1–22. https://doi.org/10.21423/TWJ.V2I1.3665.
Srivastava, A., & Anto, S. (2022). Weather Prediction Using LSTM Neural Networks. 2022 IEEE 7th International Conference for Convergence in Technology, I2CT 2022. doi: 10.1109/I2CT54291.2022.9824268.
Szalai, S., & Szinell, C. (2000). Comparison of two drought indices for drought monitoring in Hungary – a case study, in: Drought and Drought Mitigation in Europe. Springer, 161–166.
Taha, A.A., Hanbury, A., 2015. Metrics for evaluating 3D medical image segmentation: analysis, selection, and tool. BMC Med. Imaging 15 (1), 29. https://doi.org/10.1186/S12880-015-0068-X.
Taheri, M., Mohammadian, A., Ganji, F., Bigdeli, M., Nasseri, M., 2022. Energy-Based Approaches in Estimating Actual Evapotranspiration Focusing on Land Surface Temperature: A Review of Methods, Concepts, and Challenges. Energies 15 (4), 1264). https://doi.org/10.3390/en15041264.
TDOA. (2023). Texas Agriculture Stats. https://www.texasagriculture.gov/About/Texas-Ag-Stats.
Tian, L., Disse, M., Huang, J., 2023. Drought cascades across multiple systems in Central Asia identified based on the dynamic space-Time motion approach. Hydrol. Earth Syst. Sci. 27 (22), 4115–4133. https://doi.org/10.5194/HESS-27-4115-2023.
Toscano-Pulido, G., Razavi, H., Nejadhashemi, A.P., Deb, K., Linker, L., 2024. Large-Scale Multiobjective Optimization for Watershed Planning and Assessment. IEEE Transactions on Systems, Man, and Cybernetics: Systems 54 (6), 3471–3483. https://doi.org/10.1109/TSMC.2024.3361679.
TWDB. (2012). Water for Texas 2012 state water plan.
USCD. (2024). US Climate Data. https://www.usclimatedata.com/climate/texas/united-states/3213.
USDA. (2020). USDA's National Agricultural Statistics Service Texas Field Office (Part of the Southern Plains Regional Field Office). United States Department of Agriculture National Agricultural Statistics Service. https://www.nass.usda.gov/Statistics_by_State/Texas/Publications/County_Estimates/.
USDA. (2024, January 1). USDA's National Agricultural Statistics Service Texas Field Office (Part of the Southern Plains Regional Field Office) County Estimate Map - Cattle. United States Department of Agriculture National Agricultural Statistics Service. https://www.nass.usda.gov/Statistics_by_State/Texas/Publications/County_Estimates/ce_maps/ce_catt.php.
Usdm, 2023. October). What is the USDM? | U.S. Drought Monitor. https://droughtmonitor.unl.edu/About/WhatistheUSDM.aspx.
Vreugdenhil, M., Greimeister-Pfeil, I., Preimesberger, W., Camici, S., Dorigo, W., Enenkel, M., van der Schalie, R., Steele-Dunne, S., Wagner, W., 2022. Microwave remote sensing for agricultural drought monitoring: Recent developments and challenges. Front. Water 4, 1045451. https://doi.org/10.3389/FRWA.2022.1045451/BIBTEX.
Wang, Y., Liu, J., Li, R., Suo, X., Lu, E.H., 2022. Medium and Long-term Precipitation Prediction Using Wavelet Decomposition-prediction-reconstruction Model. Water Resour. Manag. 36 (3), 971–987. https://doi.org/10.1007/S11269-022-03063-X/TABLES/2.
Wei, X., Huang, Q., Huang, S., Leng, G., Qu, Y., Deng, M., Han, Z., Zhao, J., Liu, D., Bai, Q., 2022. Assessing the feedback relationship between vegetation and soil moisture over the Loess Plateau. China. Ecological Indicators 134, 108493. https://doi.org/10.1016/J.ECOLIND.2021.108493.
Wibawa, A.P., Utama, A.B.P., Elmunsyah, H., Pujianto, U., Dwiyanto, F.A., Hernandez, L., 2022. Time-series analysis with smoothed Convolutional Neural Network. Journal of Big Data 9 (1), 1–18. https://doi.org/10.1186/S40537-022-00599-Y/TABLES/12.
Wilhite, D.A., Sivakumar, M.V.K., Pulwarty, R., 2014. Managing drought risk in a changing climate: The role of national drought policy. Weather Clim. Extremes 3, 4–13. https://doi.org/10.1016/J.WACE.2014.01.002.
WMO. (2012). Standardized Precipitation Index User Guide. https://www.droughtmanagement.info/literature/WMO_standardized_precipitation_index_user_guide_en_2012.pdf.
Wong, C.I., Banner, J.L., Musgrove, M.L., 2015. Holocene climate variability in Texas, USA: An integration of existing paleoclimate data and modeling with a new, high-resolution speleothem record. Quat. Sci. Rev. 127, 155–173. https://doi.org/10.1016/J.QUASCIREV.2015.06.023.
Yamashita, R., Nishio, M., Do, R.K.G., Togashi, K., 2018. Convolutional neural networks: an overview and application in radiology. Insights into Imaging 9 (4), 611–629. https://doi.org/10.1007/S13244-018-0639-9/FIGURES/15.
Yang, Z., Gong, J., Wang, S., Jin, T., Wang, Y., 2023. Shifts bidirectional dependency between vegetation greening and soil moisture over the past four decades in China. Sci. Total Environ. 897, 166388. https://doi.org/10.1016/J.SCITOTENV.2023.166388.
Yazdandoost, F., Razavi, H., Izadi, A., 2022. Optimization of agricultural patterns based on virtual water considerations through integrated water resources management modeling. International Journal of River Basin Management 20 (2), 255–263. https://doi.org/10.1080/15715124.2021.1879093.
Zhang, B., Abu Salem, F.K., Hayes, M.J., Smith, K.H., Tadesse, T., Wardlow, B.D., 2023. Explainable machine learning for the prediction and assessment of complex drought impacts. Sci. Total Environ. 898, 165509. https://doi.org/10.1016/J.SCITOTENV.2023.165509.

Zhang, L., Yuan, F., He, X., 2024. Probabilistic Assessment of Global Drought Recovery and Its Response to Precipitation Changes. Geophys. Res. Lett. 51 (1), e2023GL106067. https://doi.org/10.1029/2023GL106067.
Zhang, Y., Liu, X., Jiao, W., Wu, X., Zeng, X., Zhao, L., Wang, L., Guo, J., Xing, X., Hong, Y., 2023. Spatial Heterogeneity of Vegetation Resilience Changes to Different Drought Types. Earth's. Future 11 (4), e2022EF003108. https://doi.org/10.1029/2022EF003108.
Zhang, Y., Wang, P., Chen, Y., Yang, J., Wu, D., Ma, Y., Huo, Z., Liu, S., 2023c. The optimal time-scale of Standardized Precipitation Index for early identifying summer maize drought in the Huang-Huai-Hai region, China. J. Hydrol.: Reg. Stud. 46, 101350. https://doi.org/10.1016/J.EJRH.2023.101350.